Utah State University

DigitalCommons@USU

All Graduate Theses and Dissertations | Graduate Studies

5-2011

Variability of Water Storage and Instream Temperature in Beaded Arctic Streams

Madeline F. Merck
Utah State University

Follow this and additional works at: https://digitalcommons.usu.edu/etd

 Part of the Environmental Engineering Commons

Recommended Citation

Merck, Madeline F., "Variability of Water Storage and Instream Temperature in Beaded Arctic Streams" (2011). *All Graduate Theses and Dissertations*. 912.
https://digitalcommons.usu.edu/etd/912

This Thesis is brought to you for free and open access by the Graduate Studies at DigitalCommons@USU. It has been accepted for inclusion in All Graduate Theses and Dissertations by an authorized administrator of DigitalCommons@USU. For more information, please contact digitalcommons@usu.edu.

VARIABILITY OF WATER STORAGE AND INSTREAM TEMPERATURE IN BEADED ARCTIC STREAMS

by

Madeline F. Merck

A thesis submitted in partial fulfillment
of the requirements for the degree

of

MASTER OF SCIENCE

in

Civil and Environmental Engineering

Approved:

Bethany T. Neilson Major Professor	Mac McKee Committee Member
Thomas B. Hardy Committee Member	Byron R. Burnham Dean of Graduate Studies

UTAH STATE UNIVERSITY
Logan, Utah

2011

Copyright © Madeline F. Merck 2011

All Rights Reserved

ABSTRACT

Variability of Water Storage and Instream Temperature

in Beaded Arctic Streams

by

Madeline F. Merck, Master of Science

Utah State University, 2011

Major Professor: Bethany T. Neilson
Department: Civil and Environmental Engineering

The purpose of this study is to investigate variation in water export and instream temperatures throughout the open water season in a beaded Arctic stream, consisting of small pools connected by shallow chutes. The goals are to better understand heat and mass movement through these systems, how this may impact chemical and biological processes, and the resulting shifts with changes in climate. This is accomplished by first examining the extent and variability of water storage and export through qualitative analysis of observational data. Further, heat fate and transport is examined through development of an instream temperature model. The model formulation, a simple approach to model calibration and validation, and information regarding residence and characteristic times of different pool layers are presented. Using temperatures measured at high spatial resolution within the pools and surrounding bed sediments as well as other supporting data (e.g., instream flow, specific conductivity, weather data, and bathymetry), various types of storage within the pools, banks, and marshy areas within

the riparian zone, including subsurface flow paths that connect the pools, were found. Additionally, data illustrated that some pools will stay stratified during higher flow periods under certain weather conditions. Through modeling efforts, the dominant heat sources were found to vary between stratified layers. It was also found that potential increases in thaw depths surrounding these pools can shift stratification and mixing patterns. These shifts can further influence mass export dynamics and instream water quality. Given the amount and different types of storage within these systems and the influence of stratification patterns on the residence times in the pools, Imnavait Basin and similar beaded Arctic watersheds will likely experience delayed export of nutrients that are limiting in most Arctic systems.

(96 pages)

ACKNOWLEDGMENTS

I would like to thank my major professor, Dr. Bethany Neilson, specifically for her patience and persistence and also for such an extraordinary opportunity. I would also like to thank my committee members, Dr. Mac McKee and Dr. Thom Hardy, not only for their time commitment but also for being the first at USU to take a chance on me. In addition to theirs was the encouragement and support of Dr. David Stevens, who graciously gave up endless hours to my constant and stubborn questioning. I must also thank Dr. George Kling for offering his expertise and time spent interpreting field data.

Thank you to Noah Schmadel, Quin Bingham, Rose Cory, Jen Kostrzewski, Jason Stuckey, Randy Fulweber, and Doug Kane for their help with data collection. Thanks also to the Inland Northwest Research Alliance, the Utah Water Research Laboratory, and the Arctic LTER (NSF-DEB 0423385) for funding this research.

Very special thanks go to my family and friends (especially Katherine!), who have been enormously supportive of my decision to return to school. Lastly and in particular, I am especially grateful to my at-home officemate, Dave Brown. Thank you for the tremendous love and support and for simply being there when I needed you.

Madeline F. Merck

CONTENTS

LIST OF TABLES

LIST OF FIGURES

CHAPTER 1

INTRODUCTION

Although mitigation of anthropogenic influences has been the historical motivation for studying instream temperatures, climate change, particularly in Arctic systems, has become the recent impetus [*Webb et al.,* 2008]. Climate change in the Arctic has resulted in seasonal increases in air temperature *[Chapman and Walsh,* 1993*; Serreze et al.,* 2000*; Wang and Key,* 2003] and changes in precipitation and wind patterns [*Hinzman and Kane*, 1992]. These changes have the potential to impact the land surface energy balance through shifts in vegetation and snowmelt patterns [*Sturm et al.*, 2005], changes in albedo and depth of thaw in soils [*Hinzman et al.*, 1991], and later freeze and earlier thaw of rivers and lakes [*Mangnuson et al.*, 2000]. All of these and other potential changes impact the hydrologic system and can therefore influence surface water temperatures.

Investigating storage and export dynamics within watersheds is important in understanding the fate and transport of heat and other constituents of interest (e.g., nutrients). Movement of heat and mass through watersheds is highly affected by storage [*McNamara et al.,* 1998] via three distinct areas including hillslope, riparian, and transient storage (lumped in-channel and hyporheic storage). Nutrient fate and transport are of particular interest in Arctic watersheds where transport is limited [*Brooks and Williams,* 1999; *Chapin et al.,* 1980; *Dowding et al.*, 1981; *Kling,* 1995; *McNamara et al.,* 2008; *Satoru et al.*, 2006], yet our current understanding of the physical processes that dictate movement within and from these storage areas is incomplete.

Hillslope storage has been thoroughly studied in the Arctic systems and is relatively well understood [*Stieglitz et al.*, 2003]. *McNamara et al.* [1997] stated that water storage is severely inhibited by permafrost, particularly in early spring when the active layer, the upper portion of the ground that experiences the freeze-thaw cycle, is at or near zero depth. They found that during snowmelt, stream flow in the Arctic is almost entirely composed of new meltwater due to the lack of hillslope storage and that pre-event water contributions to streamflow increase through the summer as thaw depths increase. *Edwardson et al.* [2003] further highlighted the importance of the active layer storage relative to increases in depth of thaw and subsequent impacts on nutrient export. As the hillslope active layer depths increase, the depths of thaw in riparian areas will also increase and create additional storage locations.

The influence of riparian areas on water and nutrient movement has been found to be important in temperate climates, especially due to flushing by rising groundwater levels [*Inamdar et al.*, 2009]. In their review focusing on the hydrologic controls of nitrogen transport in near-stream zones, *Cirmo and McDonnell* [1997] highlights the importance of these environments both biogeochemically and hydrologically in temperate climates. *Haggerty et al.* [2002] further found that long residence times due to large riparian and hyporheic storage impact the export of nutrients. Similarly, *Edwardson et al.* [2003] found that near-stream and transient storage areas within Arctic streams are biogeochemically significant. However, the hydrologic connectivity within riparian zones, between hillslope and riparian zones, and between the riparian zone and the stream are not clear. Further, the implications on storage and export of water and key materials in Arctic watersheds requires further investigation.

The influences of transient storage processes have also been investigated in the Arctic. *Zarnetske et al.* [2007] found that the greatest mean storage residence time, the average time interval that a water particle spends within a storage zone, occurred at low flow conditions and exponentially decayed with increasing discharge in alluvial and peat streams. Throughout their low flow simulations, both discharge and thaw depth correlated with transient storage, however discharge dominated storage zone conditions. More specifically, *Edwardson et al.* [2003] found the ratio of total transient storage area to channel area to be high in peat-bed beaded Arctic streams consisting of small pools connected by shallow chutes. This stream type has been known to have insignificant hyporheic exchange, but large in-pool storage due to bead volume, low discharge, and thermal stratification [*Edwardson*, 2003; *Irons and Oswood*, 1992]. While the majority of existing research on transient storage has been performed in temperate alluvial streams [*Zarnetske et al*., 2007], water storage and export within beaded Arctic streams, where stratification commonly occurs, is currently not well understood. Since headwater beaded Arctic streams are among the least studied [*Oswood et al.*, 1989] and there is only a loose understanding of the physical processes affecting both storage and instream temperature regimes, our current understanding and abilities to predict the influences of climate change in these systems are limited at best.

An improved understanding of these systems necessitates qualification of water storage and export and quantification of the heat fluxes driving stratification and in pool storage. To help achieve this, the following research objectives were developed:

Objective 1: Collect and analyze high spatial resolution data to identify the physical processes dominating or influencing beaded Arctic streams. From this

information, the extent and variability of storage and export of water and key materials due to stratification and mixing patterns within the pools in the beaded stream will be qualified.

Objective 2: Develop a method of modeling temperature stratification and mixing dynamics in individual pools with a beaded Arctic stream. This will result in a one-dimensional process based temperature model from which the dominant heat sources and sinks will be quantified through in-depth analysis of model output.

These objectives were accomplished in two separate papers. The first paper, entitled "Variability of Instream and Riparian Storage in Beaded Arctic Streams," accomplishes Objective 1 (see Chapter 2); the second paper, entitled "Modeling Instream Temperature Variability in Beaded Arctic Streams," accomplishes Objective 2 (see Chapter 3).

CHAPTER 2

VARIABILITY OF INSTREAM AND RIPARIAN STORAGE IN BEADED ARCTIC STREAMS

Abstract

The extent and variability of water storage and export throughout the open water season in beaded Arctic streams are poorly understood. Various data types were collected in Imnavait Creek, a beaded stream located north of the Brooks Range in Alaska, to better understand the effects of in-pool and riparian storage on heat and mass movement through these streams. Using temperatures measured at high spatial resolution within the pools and surrounding sediments as well as other supporting data (e.g., volumetric discharge, specific conductivity, and weather data), we found various types of storage within the pools, banks, and other marshy areas within the riparian zone, including subsurface flow paths that connect the pools. During low flow periods persistent stratification occurred within the pools due to variability in radiation penetration, presence of permafrost and low wind stress at the pool surface. Additionally, one shallow pool (<0.5m depth) had a tendency to remain stratified during higher flow periods due to cold and dense lateral subsurface flows plunging to the bottom of the pools. This consistent separation of surface and bottom water masses affected the residence times in the pools and, in this and similar Arctic watersheds, could affect the evolution of water chemistry and material export.

Introduction

The transport of materials through watersheds is highly influenced by the dynamics of water movement and storage. The rates of transport and the fate of dissolved and particulate materials in surface waters is influenced by storage areas on hillslopes, in riparian zones, and within transient storage which includes in-channel and hyporheic storage [e.g., *McNamara et al.,* 1998]. These storage areas may be particularly important for terrestrial loss and aquatic export of nutrients in tundra environments [e.g., *Brooks and Williams, 1*999; *McNamara et al.,* 2008], in part due to the extreme nutrient limitation experienced by both terrestrial and aquatic tundra ecosystems [*Chapin et al.,* 1980; *Dowding et al.,* 1981; *Kling,* 1995; *Satoru et al.*, 2006].

Hillslope storage has been thoroughly studied in the Arctic systems and is relatively well understood [*Stieglitz et al.*, 2003]. *McNamara et al.* [1997] stated that water storage is severely inhibited by permafrost, particularly in early spring when the active layer, the upper portion of the ground that experiences the freeze-thaw cycle, is at or near zero depth. They found that during snowmelt, stream flow in the Arctic is almost entirely composed of new meltwater due to the lack of hillslope storage and that pre-event water contributions to streamflow increase through the summer as thaw depths increase. *Edwardson et al.* [2003] further highlighted the importance of the active layer storage relative to increases in depth of thaw and subsequent impacts on nutrient export. For both hillslope and riparian storage zones, increases in active layer depth during summer will create additional water storage locations.

The influence of riparian areas on water and nutrient movement has been found to be important in temperate climates, especially due to flushing by rising groundwater levels [*Inamdar et al.*, 2009]. In their review focusing on the hydrologic controls of nitrogen transport in near-stream zones, *Cirmo and McDonnell* [1997] highlight the importance of these environments both biogeochemically and hydrologically in temperate climates. *Haggerty et al.* [2002] further found that long residence times due to large riparian and hyporheic storage impact the export of nutrients. Similarly, *Edwardson et al.* [2003] found that near-stream and transient storage areas within Arctic streams are biogeochemically significant. However, the hydrologic connectivity within riparian zones, between hillslope and riparian zones, and between the riparian zone and the stream are not clear. Further, the implications on storage and export of water and key materials in Arctic watersheds requires further investigation.

The influences of transient storage processes have also been investigated in the Arctic. *Zarnetske et al.* [2007] found that the greatest mean storage residence time, the average time interval that a water particle spends within a storage zone, occurred at low flow conditions and exponentially decayed with increasing discharge in alluvial and peat streams. Throughout their low flow simulations, both discharge and thaw depth correlated with transient storage, however discharge dominated storage zone characteristics. More specifically, *Edwardson et al.* [2003] found the ratio of total transient storage area to channel area to be high in peat-bed beaded Arctic streams consisting of small pools connected by shallow chutes. This stream type typically has insignificant hyporheic exchange, but large in-pool storage due to bead volume, low discharge, and thermal stratification [*Edwardson*, 2003; *Irons and Oswood*, 1992]. While

the majority of existing research on transient storage has been performed in temperate alluvial streams [*Zarnetske et al*., 2007], the temporal and spatial extent of water storage and export within beaded Arctic streams where stratification commonly occurs is unknown.

To investigate the influences of various storage mechanisms on water movement in a peat-bed beaded Arctic watershed, we collected various data types in the riparian areas (primarily in-bank or near-stream) and within two small pools. We present these data along with other information regarding the hydrologic conditions of our study site. We explor the storage and flow patterns in the riparian and in-pool areas under dry, transient, and wet conditions. We also investigated the hydrologic connectivity of the hillslope water tracks, riparian areas, and stream, and demonstrate the extent and variability of instream storage due to stratification patterns within the pools.

Site Description

This study investigates various types of storage in the Imnavait Creek sub-basin, located in Imnavait Basin in the Greater Kuparuk Watershed. Imnavait Creek flows north into Toolik River, which flows into Kuparuk River and then into the Arctic Ocean. These river basins are located north of the Brooks Range on the north slope of Alaska (Figures 2-1 and 2-2). Imnavait Creek is a beaded stream (Figure 2-3) which form when massive ground-ice deposits are exposed due to erosion by the stream [*McNamara et al.*, 1998].

This part of Alaska is wetland tundra and is completely underlain by several hundred meters of permafrost [*Osterkamp and Payne*, 1981], or permanently frozen ground. The top layer of soil, an organic peat layer 10-50 cm thick, overlies glacial till

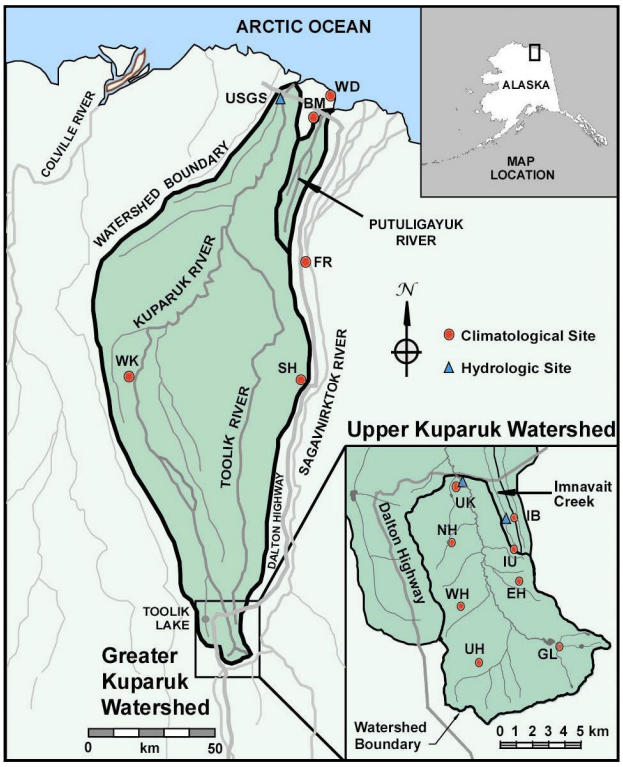

Figure 2-1. Greater Kuparuk Watershed showing the location of Imnavait Creek. (Courtesy of Doug Kane)

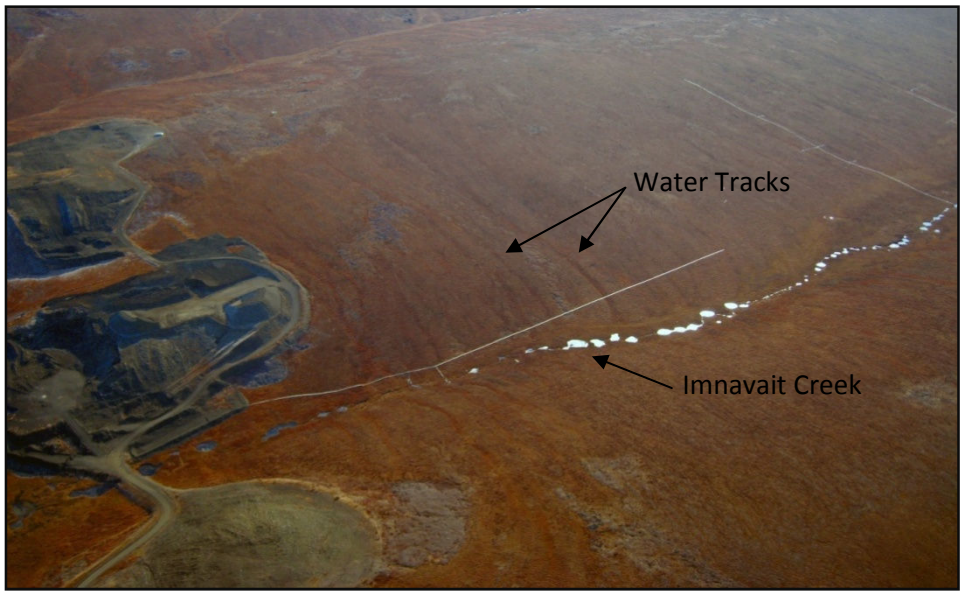

Figure 2-2. Aerial view of Imnavait Creek showing water tracks. (Courtesy of Doug Kane)

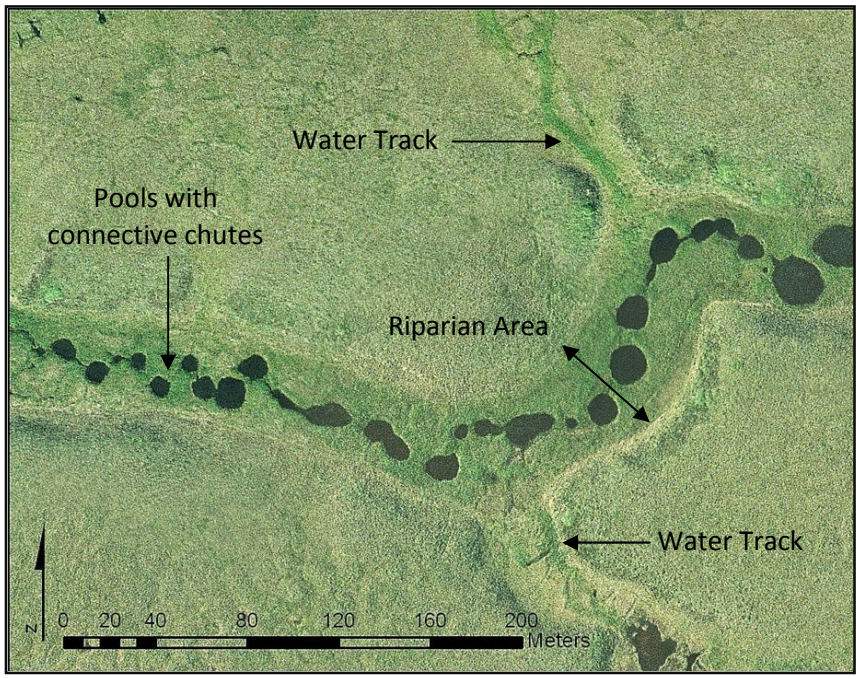

Figure 2-3. Aerial view of an example of a beaded stream showing pools and connective chutes. Also clearly delineated is the low gradient marshy area adjacent to the pools and chutes, which we consider to be the riparian area. (Photo by Torre Jorgenson)

[*Hinzman et al.*, 1991]. The active layer, typically reaches depths of approximately 25-40 cm in this area, though depths of up to 100 cm have been recorded [*Hinzman et al.*, 1991]. This area is effectively isolated from deep groundwater as the only subsurface storage and flow occurs in the shallow active layer [*Edlund et al.,* 1990]. Although precipitation events and the associated surface and subsurface runoff do occur during the summer season, the local hydrology is dominated by ablation of the snowpack [*Kane et al.*, 1989]. *McNamara et al*. [2008] found streamflow during the snowmelt to account for an average of 31-39% of the annual water flux whereas the largest summer storm events produce 3-19% of the annual water flux. They also found snowmelt streamflow to account for the highest nutrient flux though contributions from summer storm events increase during the early portion of the season with increasing depth of thaw. Water from

precipitation events flows down slope as both overland and subsurface flow through water tracks. Once the water reaches the riparian zone, the low gradient marshy area adjacent to the pools and chutes, it enters Imnavait Creek as both surface and diffuse subsurface flow through the active layer [*Kane et al.*, 2000] (Figures 2-2 and 2-3).

The portion of Imnavait Creek included in the initial 2009 study is a reach of approximately 130 meters (measured along the thalweg) that includes 6 pools and accompanying connective chutes, and 5-6 water tracks (Figure 2-4a). The pools range in surface area from 17-155 m^2 and 0.25-2.4 m in depth. The first stage of the data collection was a preliminary four day intensive field study, followed by a one month less

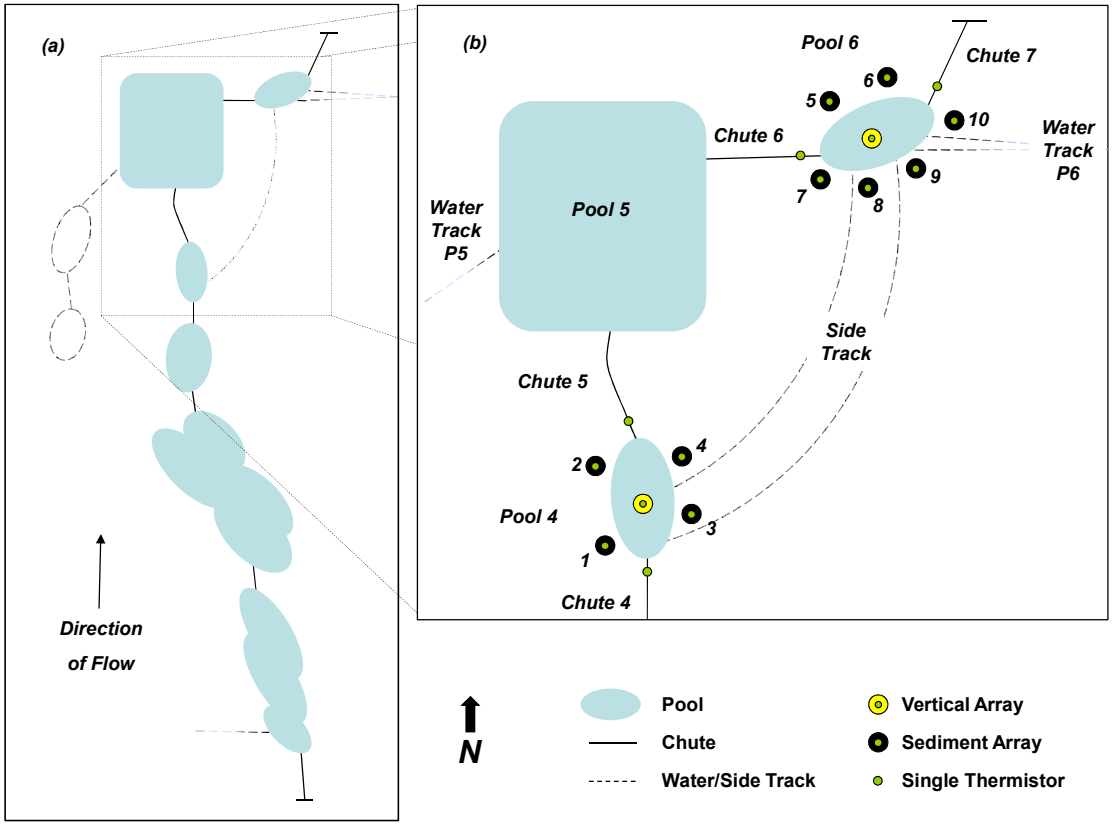

Figure 2-4. Site schematic of (a) initial study reach from 2009 and (b) smaller reach from 2010; locations of field temperature measurements are shown.

intensive study, performed from mid July to mid August, 2009. These data showed the pools were highly stratified and the flow within the system was not simple or straightforward. However, the resolution of the data did not provide adequate heat, mass, or flow balance information. Therefore, it was determined that a second stage of the study would be necessary.

The second stage was modified based on these results and occurred from early July to late August, 2010. Again, a one week intensive study was followed by a one month less intensive study. From the first stage, it was determined that higher spatial resolution data needed to be collected in order to obtain more detailed information on specific processes within the pools and surrounding areas. Therefore, the second stage was performed on a subset of pools and chutes from the previous study area (Figure 2-4b). Pools 4 and 6 were selected as data collection sites for the second stage because they are of similar size (with surface areas of 8-11 m^2 at depths of 0.35-0.5 m) and in close proximity to one another, but experience different hydro and thermal dynamics. Pool 4 appeared to be simple (a control, so to speak) with one inlet and one outlet chute. Pool 6 had more complexity, including multiple water tracks that directly connect the hillslope to the pool and enter at various temperatures along with the inlet and outlet chutes.

The spring-melt break-up peaked in this area toward the end of May, 2010. By 1 July, the first day of our 2010 field study, there had been no precipitation in over two weeks, but there had been 52.4 mm since the beginning of the year (Figure 2-5a). The air temperatures had been, for the most part, above freezing since mid May (Figure 2-5b). This weather resulted in dry upland and riparian area conditions and, therefore, very low instream flows. However, on 5 July, the rain began and persisted until the end of August.

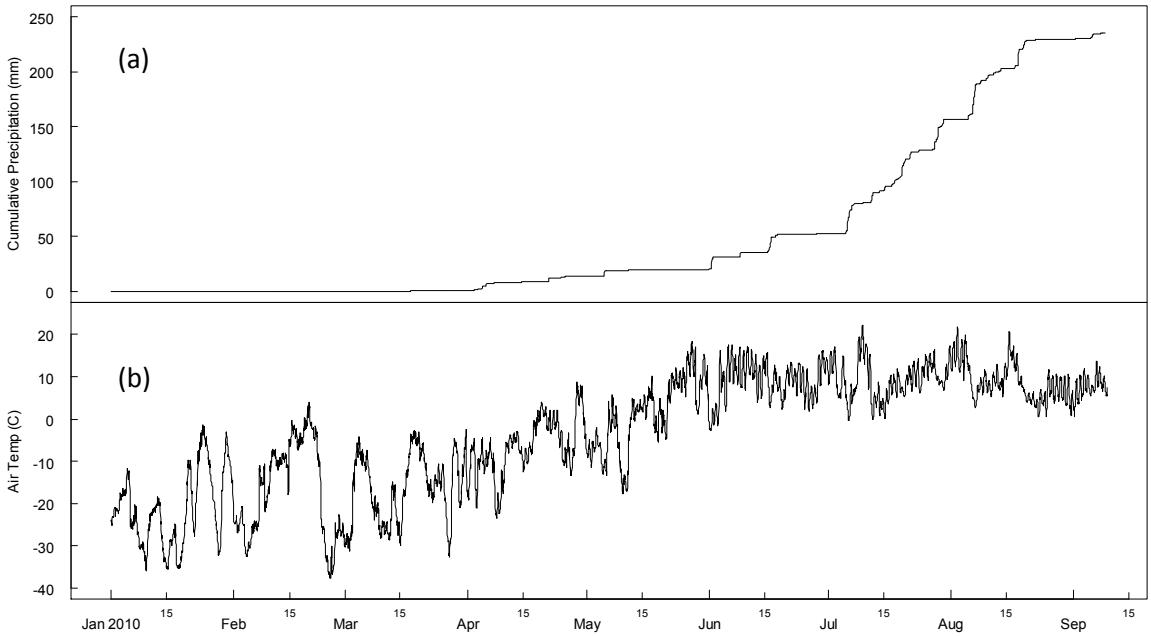

Figure 2-5. Cumulative precipitation (a) and air temperature (b) in leading up to the field study.

This nearly continuous precipitation resulted in very little available hillslope storage, running water tracks, high instream flows, elevated water surfaces and eventually a saturated riparian area.

Methodology

Hydrologic Connectivity

Due to the variation in flow and the constantly changing wetted perimeter of the connective chutes throughout the one week intensive study period, three measurement types were used to estimate discharge depending on water velocity, volumetric flow, and pool levels. The first several days of the study were relatively dry and sunny; stream velocities were low and not easily measurable. This low flow situation necessitated flow measurements using the bucket method with a 1 liter beaker capturing water flowing over

simple weirs that were installed at the inlet and outlet of each pool. When the weather turned and stream flow increased substantially, the small weirs became overtopped and were rendered useless. These high flows were then measured using the velocity-area method with a Marsh McBirney® Flo-Mate™ 2000 (Frederick, MD) (accuracy = 2% of reading) flow meter at locations where the flow merged into a relatively uniform portion of the inlet and outlet chutes. Once the high flows had been maintained long enough such that the pools were believed to be completely mixed, tracer injection studies were used to measure flows in areas where the chute geometry did not allow for measurement using the velocity-area method. Salt tracer studies were performed to calculate inlet and outlet flows using specific conductivity measurements made with a YSI® Sonde 600 LS or 600 XLS (Yellow Springs, OH) (accuracy = 0.5% of reading). These measurements were translated to chloride mass based on a linear chloride-conductivity relationship established for Imnavait Creek in 2009. A stage-discharge relationship was then determined using data from the in pool depth measurements and chute flow measurements to produce a flow time series. The stage, or pool water surface elevation, used for the stage-discharge relationship was measured using an YSI Sonde 600 LS with a vented cable in order to correct for changes in atmospheric pressure. With this information we were able to compare inlet versus outlet flows in both pools, but still were not able to explain all discrepancies due to measurement errors and limitations in information used to establish the rating curves. Further confounding our understanding, a preferential flow path (or side track) was identified that short-circuits pool 5 (Figure 2-4b). This flow path included both surface (during wet conditions) and subsurface (during both wet and dry conditions) flows depending on water levels in the riparian corridor.

To further investigate the hydrologic connectivity of this study area, spatially and temporally distributed water samples were extracted from the pools and chutes and within the surface and subsurface water in the water track and side track. A 20 cm steel needle was inserted into either the surface flow stream or 10-20 cm into the soil and approximately 40 mL of liquid was extracted. Specific conductivity and temperature were then measured using a Consort K912, which has an accuracy of 0.5% full scale of range and a resolution of 0.01 μS/cm and 0.1˚C.

Riparian Storage

Soil temperature vertical arrays were installed to establish wetting and drying patterns in the soils surrounding the pools in the riparian zone (Figure 2-4b). Onset® HOBO Water Temp Pro V2™ (Bourne, MA) (accuracy = 0.2 ºC over 0 to 50 ºC and resolution = 0.02 ºC at 25 ºC). temperature sensors were used to record the temperature in the sediment every 5 minutes. The installation methods and depths used were similar to those described in *Neilson et al.* [2009]. The sensors for these sediment temperature arrays were placed in capped and perforated 1.5" PVC pipe at depths of at 3, 9, and 20 cm (Figure 2-6). The sensors were isolated vertically from each other so as to measure temperature at a specific depth. The intent of this configuration was to allow for lateral flow through the pipe but prohibit vertical flow within the pipe. Also, by leaving the pipes in place, the sensors could then be re-installed in the same location year after year. There were 4 sediment arrays buried around pool 4 (for a total of 12 sensors) and 6 sediment arrays buried around pool 6 (for a total of 18 sensors) (Figure 2-4b).

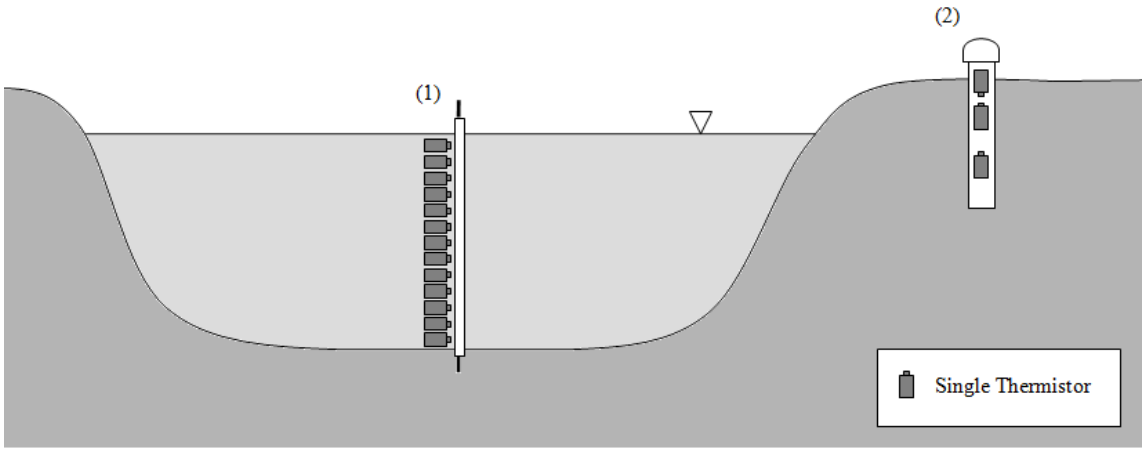

Figure 2-6. Orientation of temperature sensors in (1) vertical and (2) sediment arrays.

In-Pool Storage

HOBO Water Temp Pro V2 temperature sensors were placed vertically within pools 4 and 6 (Figure 2-4). Temperature in the water column was recorded every 5 minutes at fixed depths approximately 3 cm a part in order to capture precise timing and location of pool stratification (Figure 2-6). The 2010 vertical arrays in pools 4 and 6 included 19 and 13 sensors, respectively. The sensors were wrapped in aluminum foil to avoid heating of the sensor due to radiation penetration within the water [*Neilson et al*., 2010b]. Temperature in the water column was also verified several times throughout the second stage of the study using a Fluke® 5610™ thermistor (American Fork, UT) (accuracy = 0.01 ºC and resolution = 0.0001 ºC over 0 to 100 ºC) by measuring water temperature at 1 cm increments. These measurements were consistent with those recorded by the HOBOs verifying that the HOBO sensors were not significantly affected by solar radiation.

Additional Data Types

Several meteorological measurements were recorded on an hourly basis from a meteorological station on the west-facing ridge of the basin approximately 1 kilometer upstream of the study site. Air temperature, relative humidity, and wind speed were measured at 1, 3, and 10 meter heights using Campbell Scientific® Model 207 (Logan, UT) temperature (accuracy = 0.4 ºC over -36 to 49 ºC) and humidity (accuracy = 5% over 12 to 100%) sensors and Model 014A Met One® wind speed sensor (accuracy = 0.11 m s^{-1} over 0-45 m s^{-1}). Net solar radiation was measured using a Swissteco® Model S-1 (Oberriet, Switzerland) Net Radiometer (accuracy = 2.5% over 0.3- 60 M) and precipitation was measured at intervals of 0.1 mm using a Texas Electronics tipping bucket with an Alter windshield. A site survey was performed using a Trimble® GPS (Dayton, OH) system and included bathymetry, thaw depths, and locations of all instrumentation. Thaw depths in and around the pools were measured using a graduated probe.

Results

Hydrologic Connectivity

We found that instream flow travels from the southern portion of the study area through pool 4 and out the well defined chute continuing on to chute 5, pool 5, chute 6, and then to pool 6 or out pool 4 at the side track and on to pool 6 (Figure 2-4b). One water track flowing into pool 6 and one into pool 5 also exist, none of which were visibly running during the initial dry portion of the field study. All water tracks were saturated and flowing after several days of rain which started on 5 July.

Under dry conditions, all flows were less than 1 L s^{-1} (Figure 2-7a). Inflows to pool 4 were consistently greater than outflows suggesting a loss from pool 4 that is likely attributable to the side track. Conversely, outflows to pool 6 were greater than inflows, which is reasonable given the additional inflow from the side and water tracks. However, of particular interest is that outflows of pool 6 were less than inflows of pool 4 except under peak flow conditions, which is indicative of losses within the study reach. Once the precipitation began, instream flows increased and water levels in the pools rose, which resulted in surface flow in the side track (Figure 2-7b). Outflows from pool 6 continued to be greater than inflows, but the flow relationship for pool 4 inverted and pool 4 outflows became greater than pool 4 inflows.

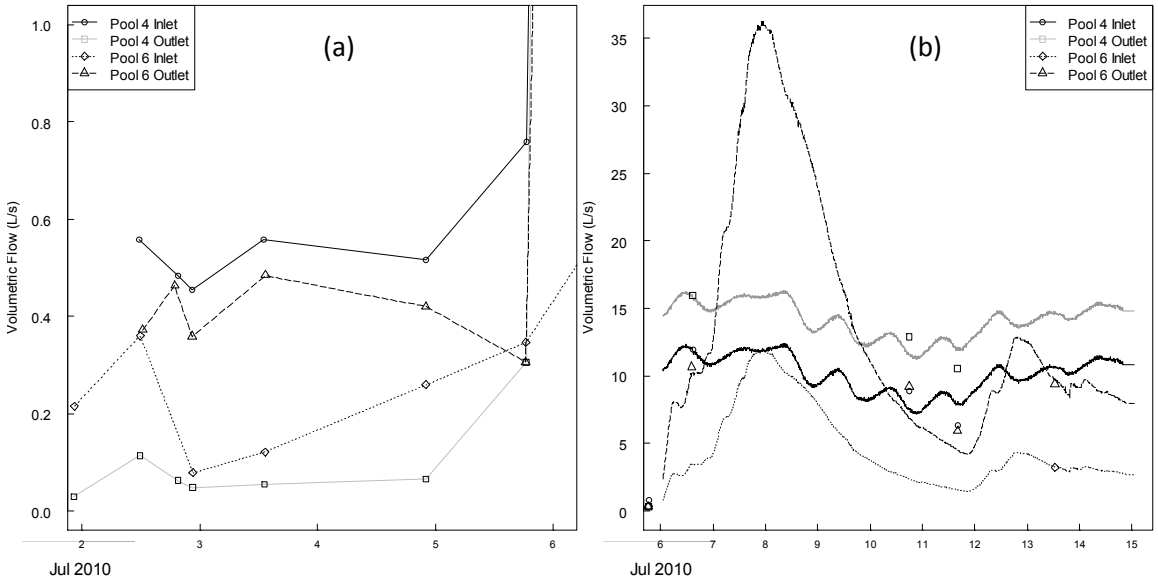

Figure 2-7. Discharge during low (a) and high (b) flows. Observations are shown as symbols and results from the stage-discharge relationship are shown as lines (high flows only).

Results of the surface water samples and soil water extraction (Table 2-1 and Figure 2-8) show that surface waters of the pools experienced measurable warming during dry low flow conditions in early July. Deeper water within the pools and subsurface flows within the side and water tracks were considerably cooler and specific conductivities were much lower. The "dry" conditions data from 2 July shows a gradual increase in the surface temperature from chute 4 to chute 6, but then a slight decrease

Table 2-1. Surface Water and Soil Moisture Extraction Grab Samples for Measurement of Temperature and Specific Conductivity at Various Locations within the Study Reach[a]

		DRY		WET			
		2-Jul		11-Aug		23-Aug	
Location Within Study Site		**Spec Cond** uS/cm	**Temp** C	**Spec Cond** uS/cm	**Temp** C	**Spec Cond** uS/cm	**Temp** C
Chute 4		498	18.9	169.1	10.4	287	7
Pool 4	Surface	501	19.2	169.5	10.3	285	7.2
	Deep	482	15.2	169.2	10.4	286	7.1
Chute 5		501	19	168.8	10.4	285	7.1
Side Track (Pool 4 Outlet)	Surface	-	-	169.2	10.4	285	7.2
	Subsurface	495	13.8	-	-	237	8
Water Track (Pool 5)	Surface	-	-	-	-	25.3	5.1
	Subsurface	-	-	-	-	78.7	5.8
Pool 5	Surface	-	-	168.3	10.3	278	7.2
	Deep	-	-	168.5	10.2	279	7.1
Chute 6		463	19.6	168.5	10.3	281	6.9
Side Track (Pool 6 Inlet)	Surface	-	-	170	10.2	275	7.5
	Subsurface	422	10.0	-	-	240	6.9
Water Track (Pool 6)	Surface	-	-	98.4	9.0	76.5	6.5
	Subsurface	178.6	10.6	-	-	103.7	7.5
Pool 6	Surface	463	19.5	169	10.3	278	7.2
	Deep	439	12.0	169.5	10.2	281	7.1
Chute 7		450	19.2	165.2	10.7	275	7.6

[a]In general, instream water is diluted and warmed as it flows through the system; more so during drier periods. During the dry period, cooler water with lower specific conductivity was found deeper in the pools and in the subsurface water. During the wet period, cooler water with lower specific conductivity was found only in the water tracks.

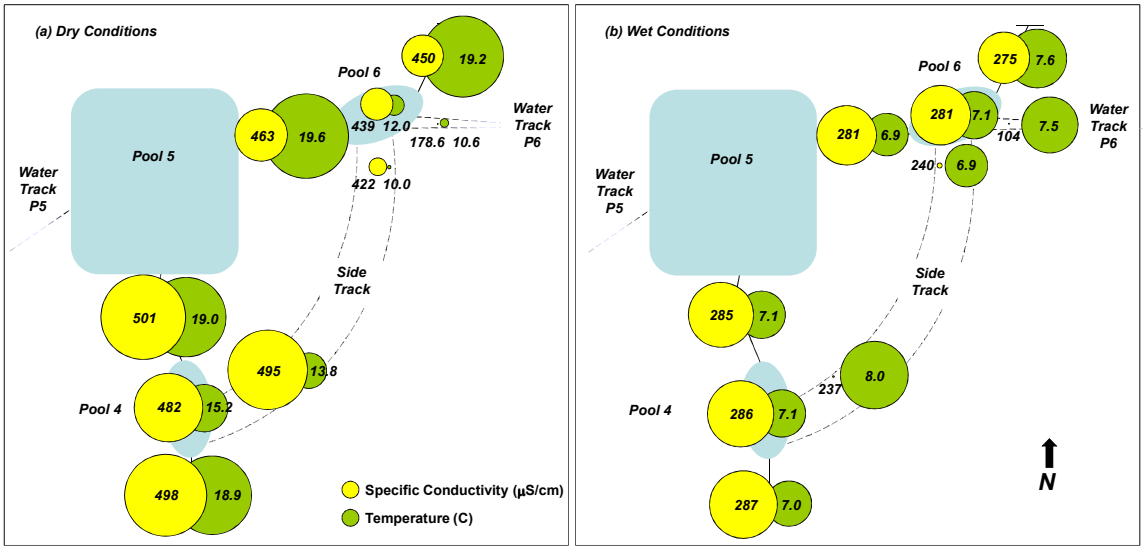

Figure 2-8. Specific conductivity and temperature of surface and soil water samples during low (a) and high (b) flows. The size of the dot is relative within each plot (a) and (b). Observations are also shown numerically at each sample location.

from chute 6 to chute 7. The surface water in pool 6 is similar to its inlet water (chute 6), however, the deeper water is considerably cooler. The temperature of the deeper water is between the pool inlet temperature and the side and water track subsurface water temperatures. The temperature of the outlet of pool 6 (chute 7) is between the temperatures of the surface and deep water within pool 6. A similar pattern is seen in the specific conductivity data for 2 July. During wet high flow conditions (11 and 23 Aug), pool temperatures and specific conductivities are much more homogeneous. However, note that for both days, the temperatures and specific conductivities of the outlet of pool 6 (chute 7) are not between the surface and deep water pool temperatures and specific conductivities. Also, on 23 August, the temperatures of the subsurface water in the water tracks are higher than their surface water temperatures due to very cold air temperatures (Figure 2-5b).

Riparian Storage

Plots of each of the 10 sediment arrays are displayed in Figures 2-9 (pool 4) and 2-10 (pool 6). Arrays #1 and #2 near pool 4 and #5 and #6 near pool 6 were on higher ground than the rest of the arrays. The sediments surrounding these arrays were initially relatively dry, but became either fully or partially saturated for the latter part of the study. Although all the arrays show strong diel temperature fluctuation in the top sensor, arrays higher elevation #1, #2, #5, and #6 initially recorded the most active and extreme fluctuations. However, notice that array #7, an array that was fully saturated throughout the entire study due to its location, started out with what might be considered the most sluggish reactions to changes in temperature and ended up with extreme reactions like the sensors in higher sediment arrays. It is thought that this top sensor diverged due to inappropriate reinstallation on 15 July resulting in temperature measurements of much shallower sediments, surface water, or air temperature fluctuations. Interestingly, it appears to dominantly mimic air temperature like the other top sensors in dry sediments. In all arrays, the middle sensors have some diel fluctuations while the bottom sensor recorded very subtle diel fluctuations. As expected, there is also a time lag in the diel fluctuations from top to middle to bottom sensors which is due primarily to conduction. In the riparian zone, the thaw depths around these pools ranged from 40 to 70 cm resulting in observed sediment temperatures that were influenced more by the atmospheric conditions rather than the frozen ground below. All sensors in all arrays became tempered once the precipitation began and the riparian area became saturated and the influences of both conduction and advection were influencing the temperature responses. For example, this occurred around 6, 12, 20, and 29 July and very obviously

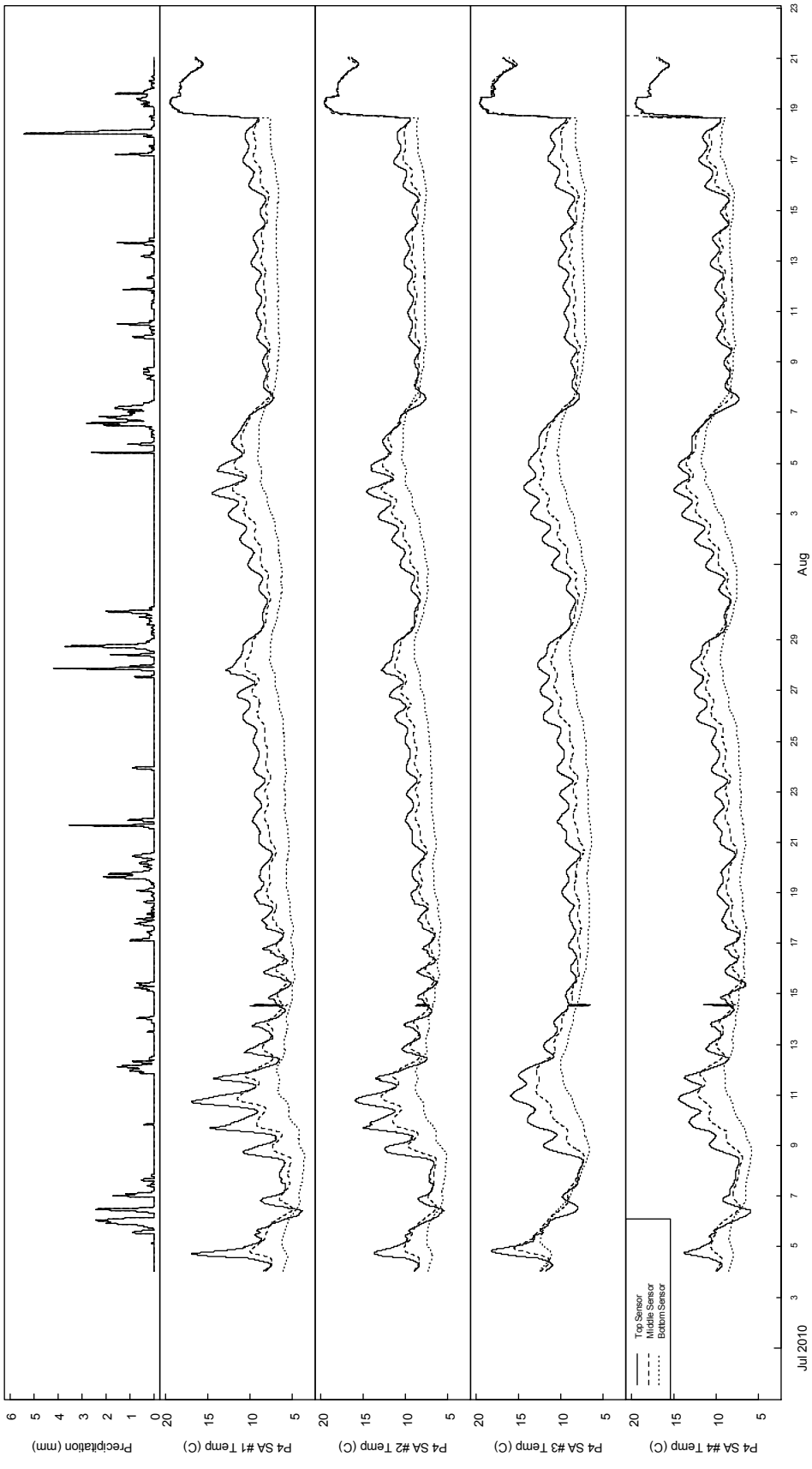

Figure 2-9. Time series of precipitation in Imnavait Basin and sediment array temperatures around pool 4. The top sensor was approximately 3 cm below the sediment surface; middle at ~9 cm; bottom at ~20 cm. See the site schematic (Figure 2-4) for array locations. Arrays #1 and #2 were initially installed in "dry" sediments and #3 and #4 were installed in "wet" sediments.

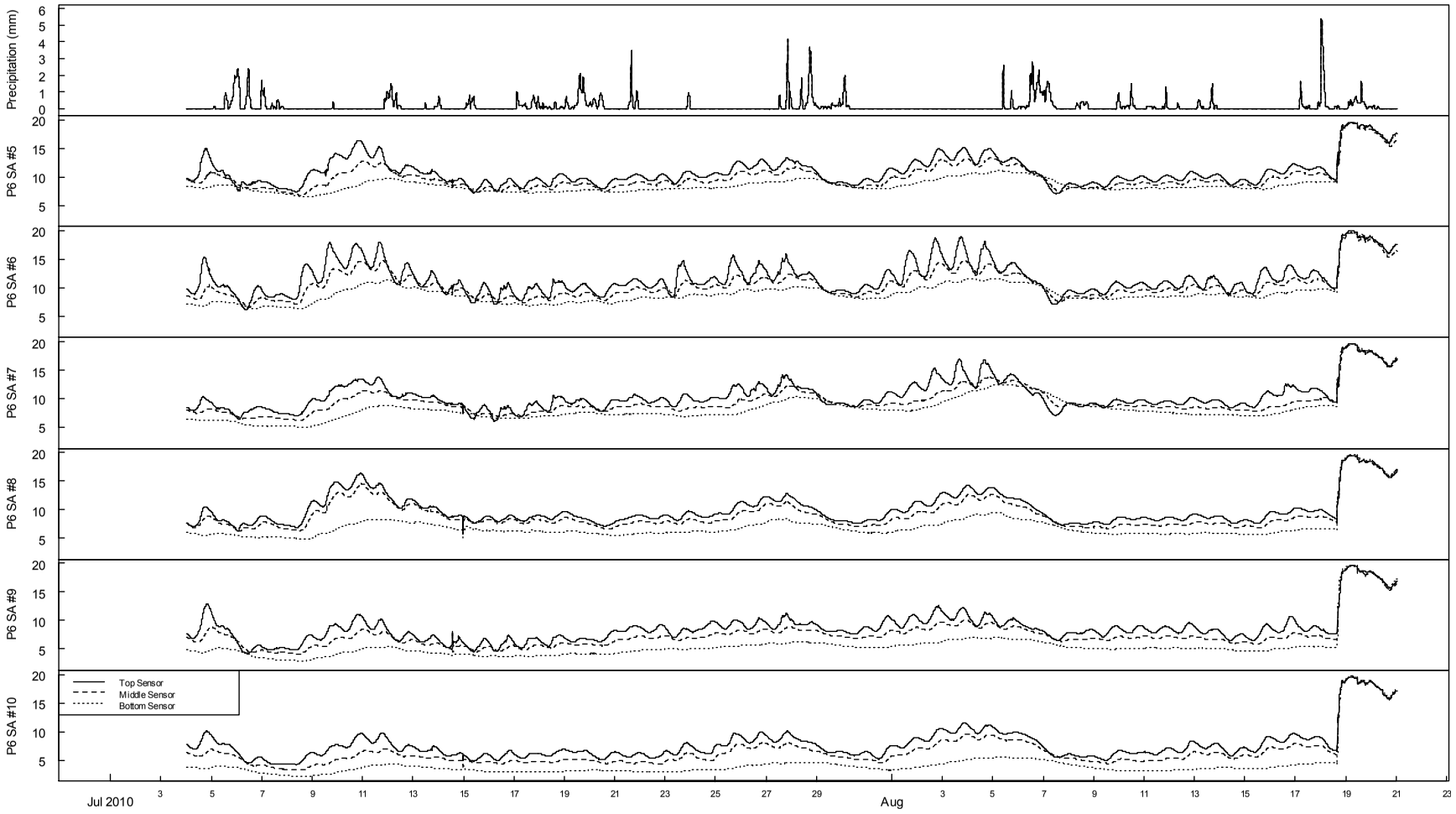

Figure 2-10. Time series of precipitation in Imnavait Basin and sediment array temperatures around pool 6. The top sensor was approximately 3 cm below the sediment surface; middle at ~9 cm; bottom at ~20 cm. See the site schematic (Figure 2-4) for array locations. Arrays #5 and #6 were initially installed in "dry" sediment and the rest were installed in "wet" sediment. Note: data from array #7 is not accurate past 15 July due to inappropriate reinstallation

around 7 August. It is important to note that conduction with the dry sediments will differ significantly between saturated ($k \approx 1.0\ Wm^{-1}K^{-1}$) and unsaturated ($k \approx 0.1\ Wm^{-1}K^{-1}$) soils [*Hinzman et al.*, 1991]. In array #6, for example, the array furthest from pool 6 both laterally and in elevation, data from the top temperature sensor in the sediment are similar to the air temperature until precipitation begins on 27 July (Figure 2-11). At that time, the sediment temperature mimics the temperature of the top layer of water in pool 6. Approximately two days after the precipitation stops, 1 August, the top layer of sediment once again responds to the air temperature. This pattern recurs with every precipitation event and is evidence of the wetting and drying of the sediments, which can drastically influence the storage and flushing of stream water and other solutes.

In-Pool Storage

At the beginning of the field study, when conditions were dry and flows were low, both pools 4 and 6 were strongly stratified throughout the entire water column during the day, although the upper portion of each pool would mix daily (Figure 2-12). When precipitation occurred, solar radiation levels and air temperature remained low (Figure 2-13), flows increased, and the pools would mix, sometimes completely. However, on 9 July, two days after the precipitation stopped, only pool 6 completely restratified (Figure 2-14). Throughout the study period, pool 6 consistently cycled between mixing and restratifying while pool 4 remained primarily mixed during high flow conditions. It is hypothesized that pool 6 restratifies more strongly due to the addition and plunging of colder water from the side and water tracks. Pool 4 does not have these additional inlet

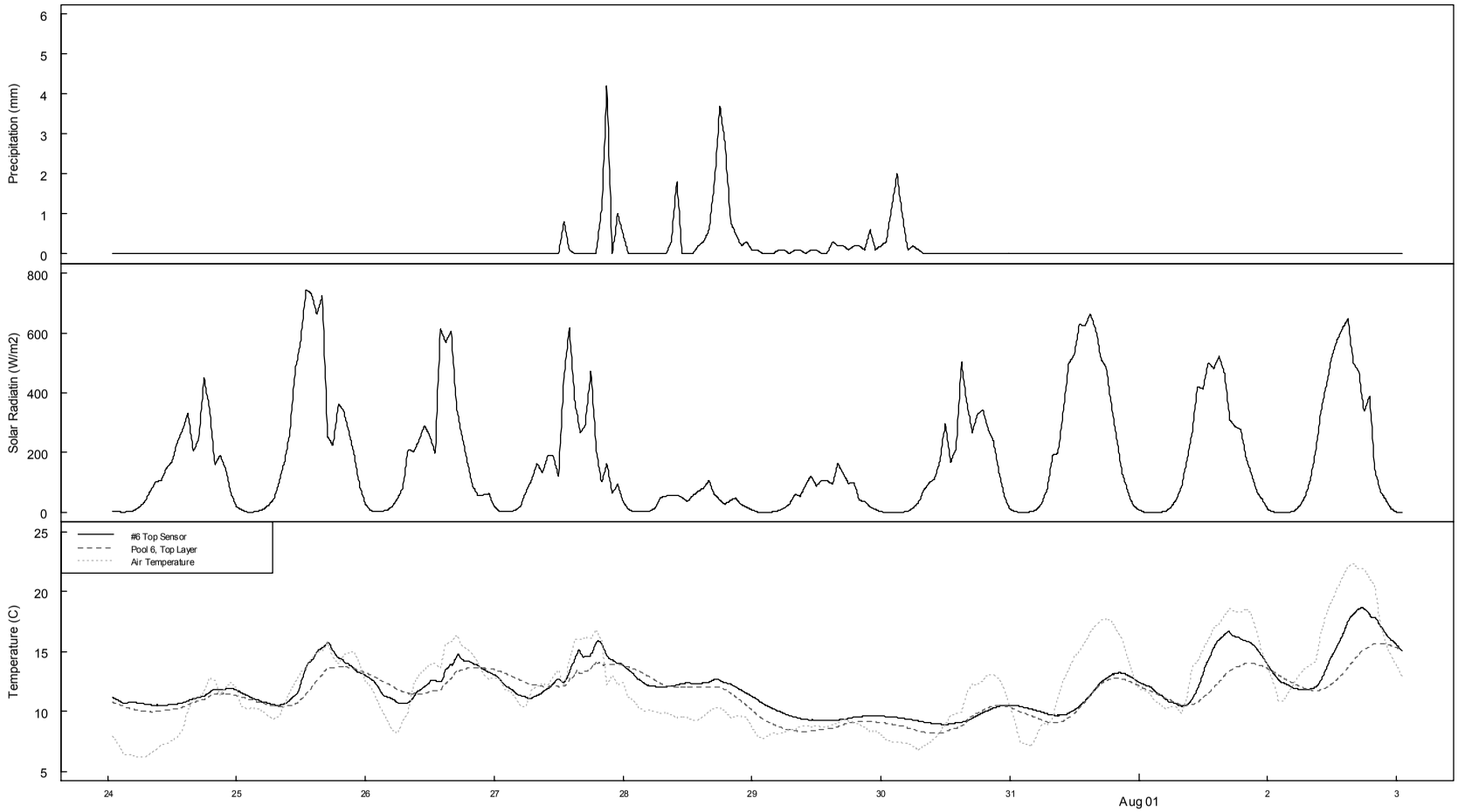

Figure 2-11. Precipitation, solar radiation, and temperatures from the 3 cm depth sensor in a "dry" sediment array from pool 6, the top layer of the water in pool 6, and the air temperature. Note the cycle of dry-wet-dry: 24-28 July (dry), 28-30 July (wet), 30 July – 3 Aug (dry). During the dry period (i.e., no precip) the solar radiation was high and the sediment temperature mimicked the air temperature. During the wet period (i.e., precip event), the solar radiation was low and the sediment temperature mimicked the top layer of the pool. It took approximately two days after the rain stopped for the sediment temperatures to once again mimic the air temperature.

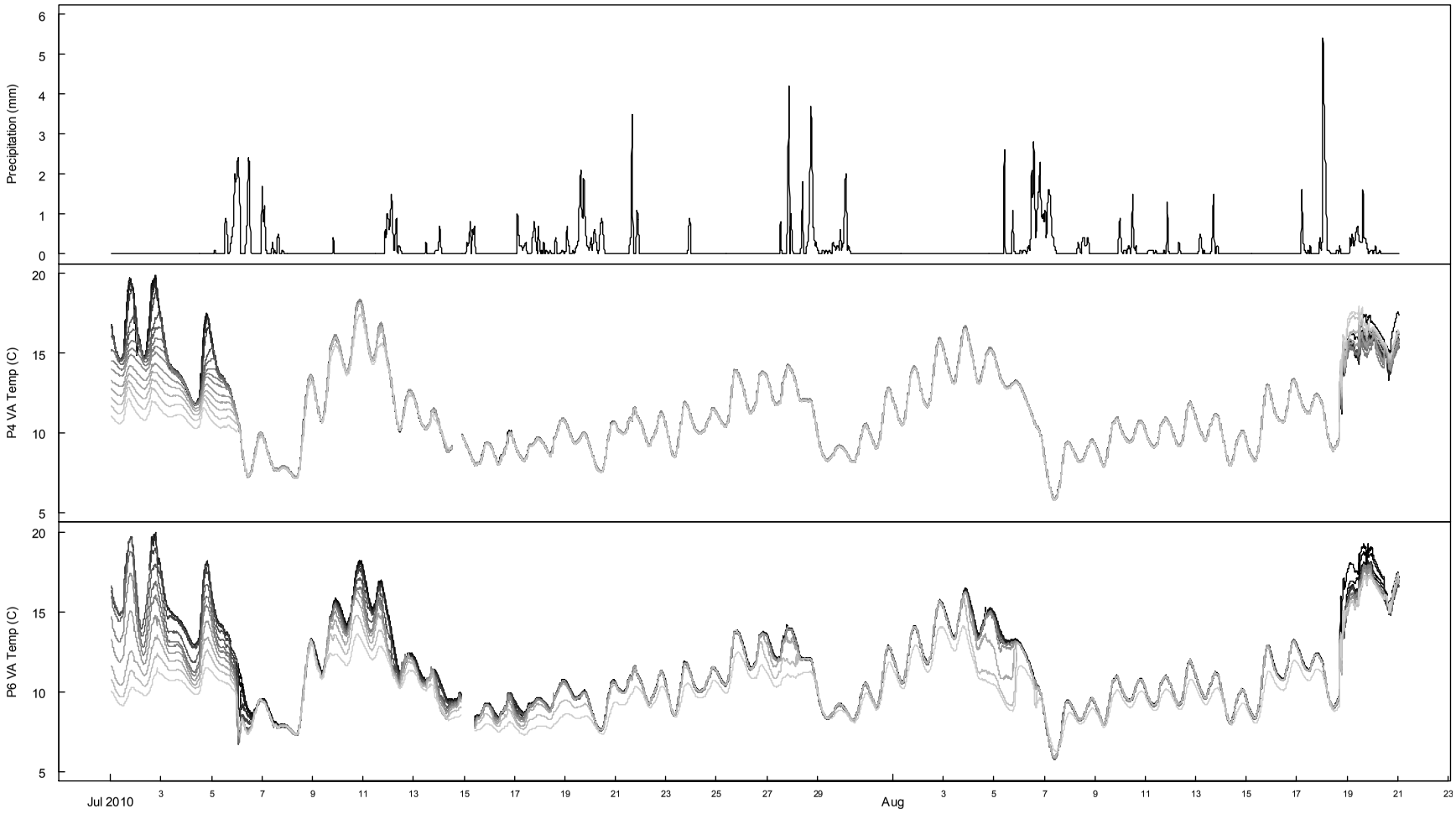

Figure 2-12. Time series of precipitation in Imnavait Basin and vertical array temperatures in pools 4 and 6. The sensors were placed every 3 cm within the water column. The darkest line represents the top sensor; subsequent lines become lighter with depth of each sensor.

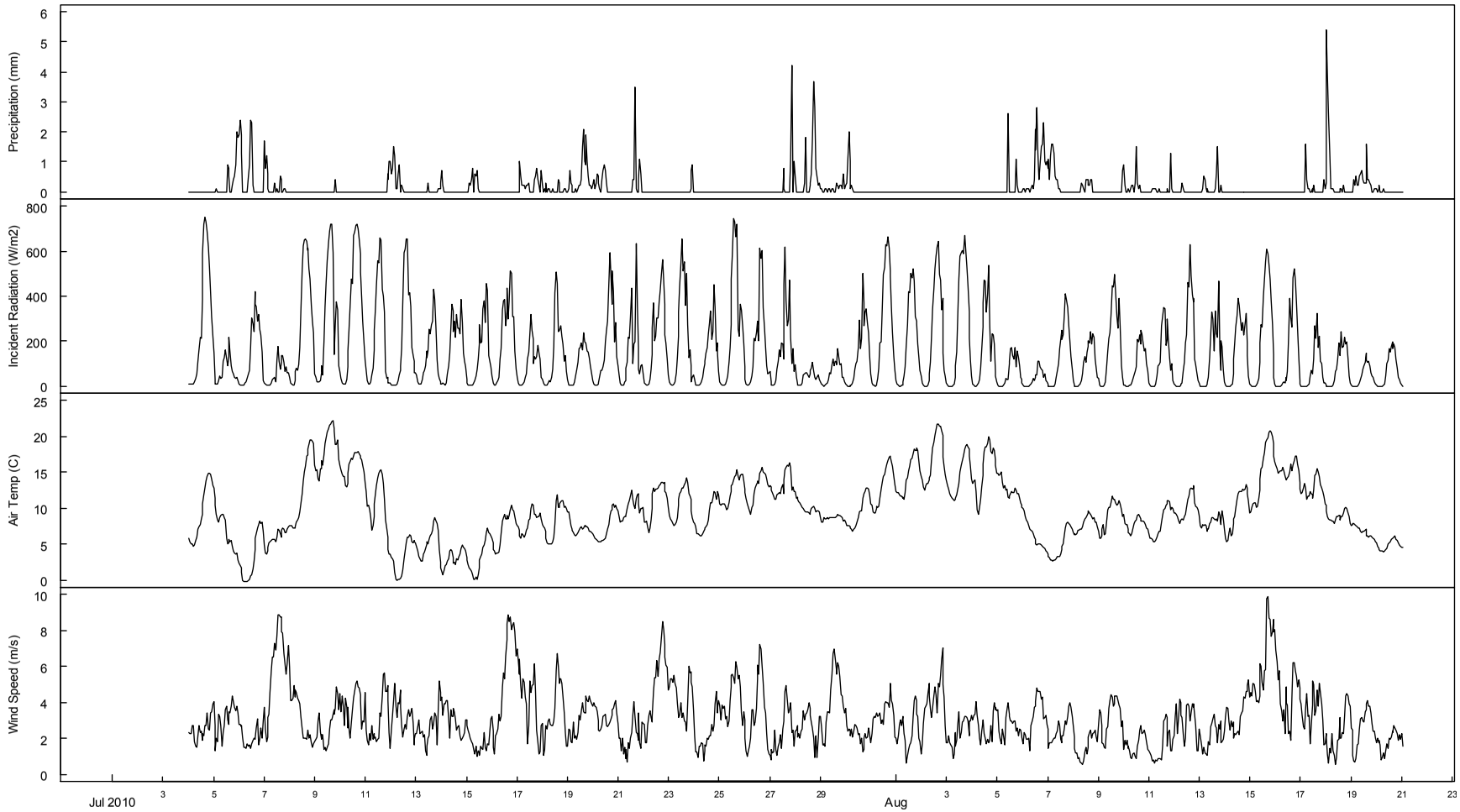

Figure 2-13. Meteorological data collected from a station on the west-facing ridge of the basin approximately 1 kilometer upstream of the study site.

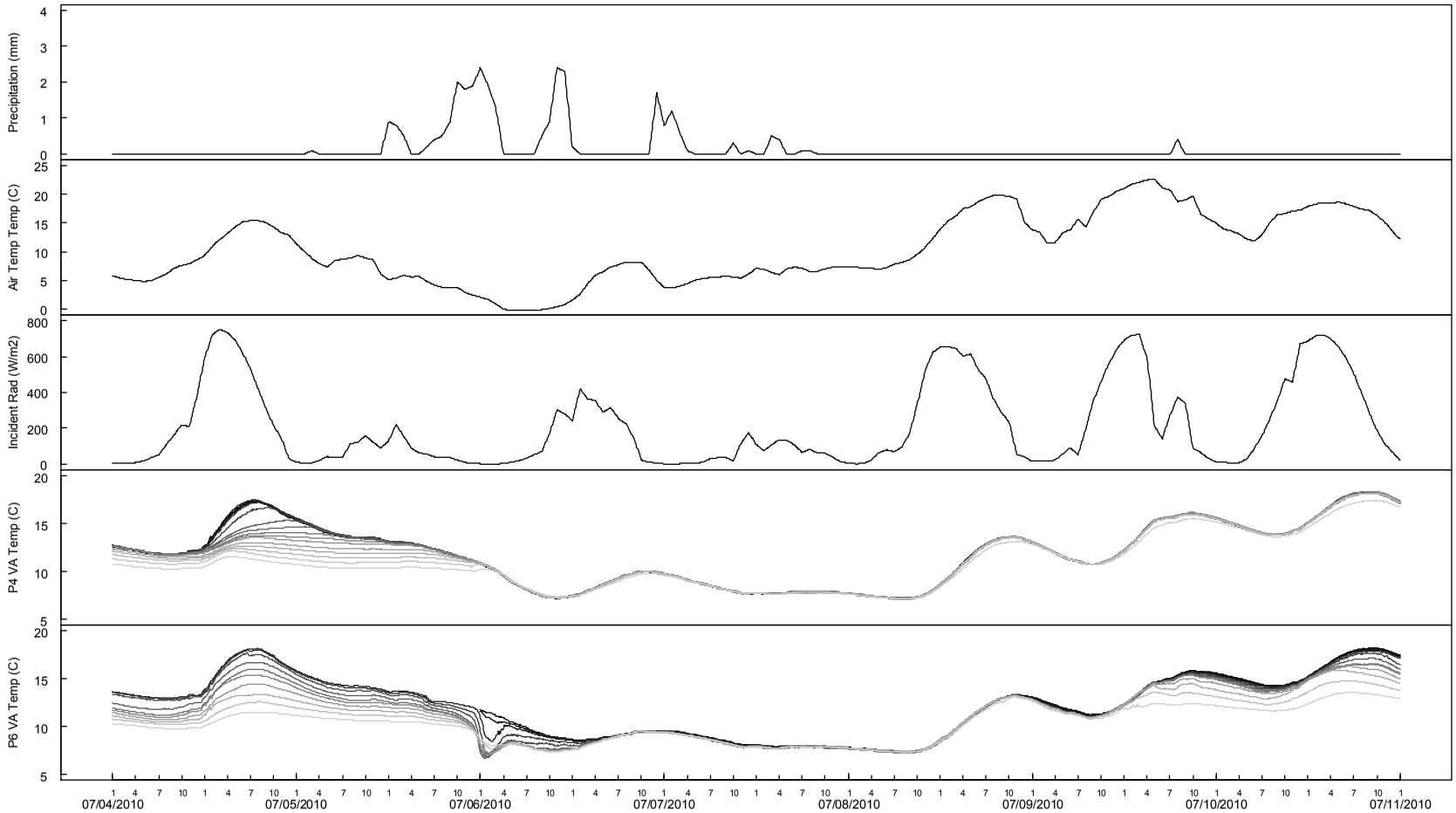

Figure 2-14. Precipitation, air temperature, solar radiation, and vertical array temperatures for pools 4 and 6. As in Figure 2-11, note the cycle of dry-wet-dry: 4-6 July (dry), 6-8 July (wet), and 8-11 July (dry). During the dry period (i.e., no precipitation) the solar radiation and air temperature were high and the pools were stratified. During the wet period (i.e., precipitation event), the solar radiation and air temperature were low and the pools became completely mixed. It took approximately two days after the rain stopped for pool 6 to restratify. Pool 4 attempted to restratify but remained primarily mixed for the remainder of the field study.

flows and, once mixed, remains mixed with the exception of minor diurnal stratification of the bottom few centimeters on 9-12 July when the flows were slightly decreased and solar radiation and air temperatures were elevated (Figure 2-13).

Discussion

At the start of the field study, the basin had been dry for several weeks (Figure 2-5). The water levels in the pools were very low, there was minimal flow within the chutes between the pools, and there was no surface flow within the water tracks (Figure 2-7a). In addition, some of the sediments surrounding the pools were dry, which is evident by comparing temperatures on 4-6 July (Figure 2-10) from sediment array #6 that was initially placed in dry sediments and sediment array #8 which was saturated throughout the study due to exit flow from the side track. At this point in time, the available hillslope and riparian storage was at its greatest. The only potential for movement of water and export of solutes laterally into the stream was due to minimal subsurface flow from melting ice lenses or permafrost thaw resulting in the small instream flows.

During this initial dry period, water exiting pool 4 at the side track was mostly surface water from the pool evidenced by specific conductivities and temperatures in the side track similar to those from the top layer of pool 4 (Table 2-1, Figures 2-8a, 2-9 and 2-12). A significant portion of the water flowing out of pool 4 would infiltrate the side track, becoming subsurface lateral flow on its path from pool 4 to 6. This loss of flow, as seen from the large disparities in inlet and outlet flows for both pools 4 and 6 during this time (Figure 2-7a), is attributable to the seemingly increasing amount of water being

stored in the side track due to its slow subsurface flow to pool 6. During its traverse from pool 4 to 6, the temperature of this subsurface lateral flow was influenced by the underlying permafrost. Once this flow reached the end of the side track it entered pool 6. Upon entering, the significantly colder water plunged, adding volume to the already cool bottom layer of pool 6 and therefore assisted in keeping the pool stratified. We anticipate that subsurface flow, and at times cold surface flow, from water tracks would have a similar effect on stratification during a variety of flow conditions.

In looking at the synoptic sampling during the dry period (2 July, Table 2-1 and Figure 2-8a), note that the water track, experiencing only subsurface flow at this point, had a relatively low specific conductivity (178.6 μS/cm). Water in the side track near pool 4 had a specific conductivity of 495 μS/cm; however, the concentration was diluted to 422 μS/cm near pool 6. This is indicative of the addition of lower specific conductivity water likely due to hillslope contributions or the residence times in the side track being long enough that the water near pool 6 was older (i.e., from a previous event).

Storage within the pools during low flow conditions was similar in nature to that of the side track riparian storage in that there was little or slowed movement of water into and out of the lower layers of these pools when stratified (Figure 2-12). Because the warmer inlet flows entered the pools within the surface layers and there was minimal advective mixing between the warm surface and cold lower layers during low flows, the inlet flows consistently skimmed the pool surface during the day (Table 2-1 and Figures 2-8a and 2-12). At night, lower air temperatures and minimal solar radiation resulted in lower temperatures of the pool's surface layer creating a diurnal mixing pattern within the upper layers. Therefore, we anticipate that the depth over which the inlet flows

mixed became deeper at night. Small amounts of exchange with the bottom layers were likely occurring due to minimal advective mixing and diffusive exchange with the water in the upper layers. Since there had been no rain in the multiple weeks prior to this data being collected, the water and accompanying solutes in the bottom layer of the pools were likely from several weeks earlier. In fact, it is highly possible that a fraction of the water in deeper pools may have been from the spring melt.

Once precipitation began on 5 July, the large amounts of available hillslope and riparian storage within the active layer started to fill. It took approximately two days before the water tracks consistently produced surface flow and instream flows started to significantly change. During this transition between dry and wet conditions, the arrays that initially had been installed in dry sediments would become completely saturated with stores of water from the rising levels of the adjacent pools, cold infiltrated rain, and lateral hillslope water (e.g., arrays #1-6 and #9 in Figures 2-9 and 2-10) [*Bense and Kooi*, 2004]. The rain, cold air temperatures, and minimal radiation (Figure 2-13) also resulted in significant cooling of the upper layers of the pools and surrounding sediments. At this time, temperatures of the pools and surrounding sediments quickly plunged and became uniform as the upper layers cooled to that of the lower layers.

On 6 July, after the rain event, the flows in pool 4 switched from inlet flows greater than outlet flows to outlet greater that inlet. The top layer of adjacent sediment became saturated as is evident by the sudden drop in temperature recorded by the top sensor in all of the sediment arrays (Figure 2-9). However, it was not until the second rain event on 12 July that the sediment became fully and continually saturated, thereby significantly increasing its thermal conductivity. At this point, all the top sediment

sensors began mimicking the top water layer temperatures rather than the air temperature (Figure 2-11).

After the transition period and filling of the active layer, the hillslope and riparian areas became completely saturated and most of the precipitation became surface runoff. All water and side tracks maintained continuous surface flow, the pools filled, instream flow increased significantly (Figure 2-7b), and all subsurface storage, including riparian storage, appeared to be at capacity. The resulting increased instream flows created turbulent conditions in the chutes and pools and further aided in mixing the layers within each pool (Figure 2-12). With nearly completely mixed conditions, the instream storage that had previously resided in the bottom layer of the pools would be exported downstream. Complete mixing of the pools was initially achieved on 7 July at a flow rate of approximately 15 L s^{-1}. Once completely mixed, we expect that all the solutes in the bottom layer became entrained in the main stream flow. With the flow rates and water surfaces elevated as they were, the export of these solutes from the pools would be relatively quick and the only remaining in-pool storage would be stagnant areas near the edge of the flooded pools.

Both surface and subsurface flow paths within our study reach changed depending on whether the hillslope and riparian areas were dry or saturated. Under dry conditions, the hydrologic connectivity of the hillslope to the riparian zone was indirect through minimal diffuse lateral flow. Saturated conditions facilitated direct hydrologic connectivity through hillslope surface runoff and surface flow in the water tracks. In some cases, the flow from the water tracks also directly connected the hillslopes to the pools within the stream.

Due to increasingly larger volumes of available storage in the active layer surrounding the stream, water from the hillslope was stored in the riparian areas before being exported to the stream as diffuse lateral flow during dry conditions. Side tracks, an additional form of storage within the riparian zone, would allow water from the pools to follow subsurface preferential flow paths during low flow conditions. Conversely, during high flow conditions, elevated surface waters would saturate the riparian area sediments and the timing of export would be delayed.

As noted by *Zarnetske et al.* [2007] and *McNamara et al.* [2008], hydrologic processes such as storage and flushing of nutrient rich waters are highly dependent on conditions such as the presence of permafrost, high occurrence of waterlogged anoxic soils, nitrogen retention in tundra environments, low annual discharge, and snowmelt. Overall, we found the extent of water storage and export in these beaded systems to be highly variable over both space and time. This variability is dependent on antecedent and changing weather conditions which influence hillslope, riparian, and in-pool storage that may in turn be influenced by global climate change.

The role of hillslope storage in Arctic systems is already relatively well understood [*McNamara et al.,* 1997; *Stieglitz et al.*, 2003], however, the hydrologic connectivity of the hillslope to the riparian zone and stream in Arctic watersheds is poorly understood. We found that the connectivity is both direct, through water tracks and runoff, and indirect, through diffuse lateral flow, and there is significant riparian storage of hillslope water. This riparian storage can subsequently influence in-pool storage through lateral flow. Conversely, when unsaturated, the available storage in the riparian zone can be influenced by exchange with instream water when pool levels

increase. Our findings of large in-pool storage due to bead volume, low discharge, and thermal stratification concur with *Edwardson et al.* [2003].

The timing of the eventual entrainment of water in various storage zones is important for nutrient export and the overall health of a watershed. Changes in the amount of water being stored and export dynamics can have basin wide effects, impacting chemical and biological rates as well as chemical concentrations downstream. These effects are particularly important in nutrient limited Arctic systems and may vary drastically given weather variability due to climate change.

Conclusion

The purpose of our study was to identify the types and patterns of storage within a beaded Arctic stream. We investigated this through tracing water flow paths in and around the study reach. Using primarily synoptic measurements of specific conductivity and time series temperature profiles, we gained insight into the patterns of wetting and drying of the riparian sediments and stratification of the pools during dry to saturated conditions.

As expected, the hydrologic connectivity of the hillslope to the riparian zone is both direct, through water tracks and runoff, and indirect, through diffuse lateral flow, and results in riparian storage of hillslope water. However, we found that riparian and hillslope storage can also subsequently influence in-pool storage through subsurface lateral flow. Conversely, when unsaturated, the available storage in the riparian zone can be influenced by exchange of instream water when water levels increase.

Dry conditions with low flows facilitated greater in-pool storage. This is primarily due to strong thermal stratification which produced large stores of cooler water with long residence times in the bottom layers of the pools. However, even under high flow conditions stratification was still observed in pools due to influences of cold lateral inflows. In the earlier portion of the thaw season, this water has the potential to be nutrient rich as the bulk of it is most likely from spring melt. Wet conditions with high flows resulted in complete or nearly complete mixing of the pools, which resulted in large volumes of instream waters flushing the long-term in-pool storage.

Our results show that the hydrologic connectivity of Arctic watersheds with beaded streams, and therefore the storage and export of water and nutrients from and within the watershed, is complex and quite dynamic. Overall, we found that the extent of water storage and export in the riparian and in-pool areas within these beaded systems are highly variable, will greatly influence the timing of material export, and potentially have cumulative impacts in the downstream higher order rivers.

CHAPTER 3

MODELING INSTREAM TEMPERATURE VARIABILITY IN BEADED ARCTIC STREAMS

Abstract

Variation in instream temperatures due to climate change may drastically affect the health and stability of aquatic Arctic ecosystems. To better understand temperature variation in these systems, the dominant heat sources and sinks must be quantified. This study examines the variability of instream temperatures in Imnavait Creek, a beaded Arctic stream consisting of small pools connected by shallow chutes, located north of the Brooks Range in Alaska. Temperature data were collected vertically within the water column of two pools and surrounding bed sediments during stratified conditions. These temperature and other supporting data (e.g., instream flow, weather data, and bathymetry) have been used to investigate heat fate and transport through the development of an instream temperature model. This model includes advective, surface, and bed conduction fluxes, simplified vertical exchange between stratified layers, and attenuation of shortwave radiation within the water column of a single pool within the stream. We present the model formulation, data collection methods used in support of model development and population, and a simple approach to model calibration and validation. We also provide information regarding residence times of different pool layers and the subsequent influence on fate and transport of heat and other constituents of interest (e.g., nutrients). We found that the dominant heat sources vary between stratified layers and,

through some simple model scenarios, that potential increases in thaw depths surrounding these pools can shift stratification, mixing patterns and instream storage dynamics.

Introduction

Although mitigation of anthropogenic influences has been the historical motivation for studying instream temperatures, climate change, particularly in Arctic systems, has become the recent impetus [*Webb et al.*, 2008]. Climate change in the Arctic has resulted in seasonal increases in air temperature [*Chapman and Walsh*, 1993; *Serreze et al.*, 2000; *Wang and Key*, 2003] and changes in precipitation and wind patterns [*Hinzman and Kane*, 1992]. These changes have the potential to impact the land surface energy balance through shifts in vegetation and snowmelt patterns [*Sturm et al.*, 2005], changes in albedo and depth of thaw in soils [*Hinzman et al.*, 1991], and later freeze and earlier thaw of rivers and lakes [*Mangnuson et al.*, 2000]. All of these and other potential changes impact the hydrologic system and therefore can influence surface water temperatures.

The effects of changing climate on surface water temperatures are of particular interest in the Arctic due to the sensitivity of low energy environments and cold region processes [*Rouse* et al., 1997]. Due to smaller water volumes, headwater beaded Arctic streams are more sensitive to climate and surrounding topography. As shown in Chapter 2, the hydrologic connectivity of hillslope and riparian areas in small headwater beaded Arctic streams is dynamic and can influence instream heat budgets. These streams experience high instream temperatures, periodic thermal stratification of the pools [*Irons and Oswood*, 1992], and are significantly influenced by the presence of underlying

permafrost. To understand the temperature dynamics in these systems, these unique characteristics require a more precise definition of the energy budget and inclusion of energy flux terms that may otherwise be ignored [*Brown*, 1969]. Since headwater beaded Arctic streams are among the least studied [*Oswood et al.*, 1989] and there is only a loose understanding of the physical processes affecting the instream temperature regimes, our current abilities to predict the influences of climate change in these systems are limited at best.

Models can be used to estimate the potential effects of climate change on various interdependent physical, chemical, and even biological processes of a water body [*Rouse et al.*, 1997; *Vorosmarty et al.*, 2001]. When predicting water temperatures, the modeling approaches used within streams and lakes are similar. Stream temperature models are most often deterministic, one-dimensional in the longitudinal direction, and apply heat and mass balances to completely mixed reaches within the river. The energy balances within these models include advection and surface fluxes (e.g., QUAL2E [*Brown and Barnwell*, 1987]), though some also include shading corrections, streambed conduction, topographic and riparian vegetation radiation, and stream friction (e.g., Heat Source [*Boyd and Kasper*, 2004] and SNTEMP [*Theurer et al.*, 1984]). Lake or reservoir models are also often one-dimensional, but exchange occurs in the vertical direction. These typically apply mass and energy balances to uniform, completely mixed horizontal layers. They also include surface fluxes in the top layer and apply turbulent diffusivity to exchange heat and mass between layers (e.g., CEQUAL-R1 [*Environmental Laboratories*, 1990] and LAKE2K [*Chapra and Martin*, 2004]).

Modeling performed on water bodies possessing characteristics of both streams and lakes, like beaded streams, must account for site specific combinations of processes [*Caissie*, 2006]. In this paper, a method of modeling instream temperatures was developed for a small headwater beaded Arctic stream based on site specific observational data and a combined stream/lake modeling approach. This resulted in a one-dimensional process based temperature model that allows for the quantification of heat fluxes during steady flow conditions. We present the model formulation, data collection methods used to support the modeling approach, a simple approach to model calibration and validation, and information regarding the dominant heat fluxes within each layer. Using the calibrated model, we then provide information regarding residence times of different pool layers and the subsequent potential influence on the fate and transport of heat and other constituents. Finally, we illustrate some model scenarios based on potential climate change impacts.

Model Formulation

One of the most effective techniques for predicting the influence of various heat sources and sinks on instream temperature is to use an energy budget [*Brown*, 1969]. Along these lines and similar to other lake and reservoir models, this model subdivides the pool and adjacent sediments into three horizontal layers with heat exchange between the pool layers (Figure 3-1). The bottom layer of sediment is further divided into discrete layers in order to apply a finite divided differences scheme [*Chapra and Canale*, 2006] to solve for heat transfer due to conduction from the bottom layer of the pool to the permafrost. Since the riparian sediments adjacent to the top two layers of the pool are

typically not frozen during the open water season, a simplified estimate of bed conduction is applied based on measured boundary condition temperatures at known distances from the pool edge. Sources and sinks of heat in the overall energy budget include: advection in the top pool layer; surface fluxes across the air-water interface of the top pool layer (J_{an}, J_{sn}, J_{br}, J_e, and J_c); attenuation of shortwave radiation within the water column of all three pool layers; bed conduction between the pool and associated sediment layers (J_{bed}); and vertical exchange between pool layers (Figure 3-1).

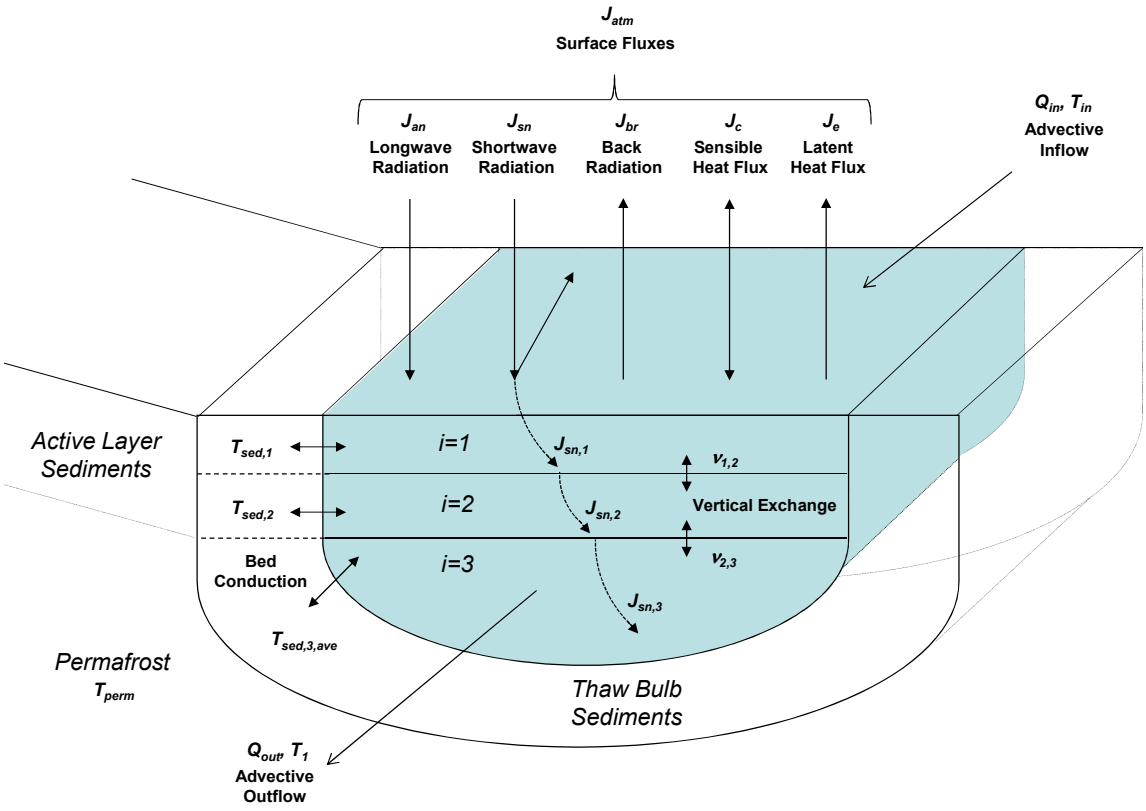

Figure 3-1. Conceptual model of the pool showing advective inflow and outflow, surface fluxes, sediment fluxes, attenuation of shortwave radiation, and pool and sediment layers.

The model assumptions include completely mixed layers within the pool; isotropic sediment thermal properties; advection in the top layer only (i.e., no plunging) due solely to volumetric inflow and outflow (i.e., no advective mixing); heat transfer between pool layers based on a simple exchange formulation presented within *Chapra* [1997] due to small surface area, short fetch, and high, protective banks; simplified estimates of bed conduction between sediments and associated pool layers; and constant volume of all layers.

The heat balance resulting from these assumptions can then be written for each layer of the pool (see the Appendix for full derivation):

Pool Layer 1:

$$\frac{dT_1}{dt} = \frac{Q_{in}T_{in}}{V_1} - \frac{Q_{out}T_1}{V_1} + \frac{J_{atm}A_{s,1}}{\rho_1 C_p V_1} - \frac{\nu_{1,2}A_{s,2}}{V_1}(T_1 - T_2) - \frac{K_{sed}A_{s,sed,1}\left(T_1 - T_{sed,1}\right)}{\rho_1 C_p V_1 z_{sed,1,2}} \quad (1)$$

Pool Layer 2:

$$\frac{dT_2}{dt} = \frac{J_{sn,2}A_{s,1}}{\rho_2 C_p V_2} + \frac{\nu_{1,2}A_{s,2}}{V_2}(T_1 - T_2) - \frac{\nu_{2,3}A_{s,3}}{V_2}(T_2 - T_3) - \frac{K_{sed}A_{s,sed,2}\left(T_2 - T_{sed,2}\right)}{\rho_2 C_p V_2 z_{sed,1,2} 1.5} \quad (2)$$

Pool Layer 3:

$$\frac{dT_3}{dt} = \frac{J_{sn,3}A_{s,1}}{\rho_3 C_p V_3} + \frac{\nu_{2,3}A_{s,3}}{V_3}(T_2 - T_3) - \frac{K_{sed}A_{s,sed,3}\left(T_3 - T_{sed,3,ave}\right)}{\rho_3 C_p V_3 z_{sed,3} 0.5} \quad (3)$$

The subscripts *1*, *2*, *3*, *in*, *s*, *perm*, *atm*, *sed*, and *ave* specify the top, middle and bottom layer of the pool or sediment, inflow, surface, permafrost, atmospheric, sediment, and average, respectively. These equations were solved numerically using Euler's Method. Using a finite divided-difference method [*Chapra and Canale*, 2006], the heat balance for the sediment volume below the pool with *n* incremental layers is:

Sediment Top Layer, n=1:

$$\frac{dT_{sed,1}}{dt} = \frac{\alpha_{sed}\left(2T_3 - 5T_{sed,2} + 4T_{sed,3} - T_{sed,4}\right)}{\Delta z_{sed}{}^2} \tag{4}$$

Sediment Layers n=2 to n-1:

$$\frac{dT_{sed,n}}{dt} = \frac{\alpha_{sed}\left(T_{sed,n-1} - 2T_{sed,n} + T_{sed,n+1}\right)}{\Delta z_{sed}{}^2} \tag{5}$$

Sediment Bottom Layer, n=n:

$$\frac{dT_{sed,n}}{dt} = \frac{\alpha_{sed}\left(2T_{perm} - 5T_{sed,n} + 4T_{sed,n-1} - T_{sed,n-2}\right)}{\Delta z_{sed}{}^2} \tag{6}$$

where T = temperature (℃), Q = volumetric flow rate (m^3 day^{-1}), V = volume of the layer (m^3), ρ = density of the water (g m^{-3}), C_p = heat capacity of the water (cal g^{-1} ℃$^{-1}$), A_s = surface area of each layer of the pool (m^2), ν = the vertical heat transfer coefficient (m day^{-1}), K = thermal conductivity of the sediment (cal m^{-1} ℃$^{-1}$ day^{-1}), α_{sed} = thermal diffusivity of the sediment (m^2 day^{-1}), z = depth (m), Δz_{sed} = incremental depth of the sediment used in the finite difference calculations (m), J_{atm} = total surface flux (cal m^{-2} day^{-1}), $J_{sn,i}$ = shortwave solar radiation (cal m^{-2} day^{-1}) of each layer due to attenuation and is defined as

$$J_{sn,i} = J_{sn} e^{\lambda_i z_i} \tag{7}$$

where J_{sn} = net measured incoming less reflected shortwave solar radiation (cal m^{-2} day^{-1}) and λ_i= broad spectrum shortwave solar radiation attenuation coefficient for each layer (i) (m^{-1}). The total surface flux (J_{atm}) is further defined as

$$J_{atm} = J_{sn,1} + J_{an} - J_{br} - J_c - J_e \tag{8}$$

Note that the total surface flux term is only applicable to the top pool layer (i=1) and therefore only includes $J_{sn,1}$. The remaining surface flux terms, J_{an} = net atmospheric longwave radiation, J_{br} = longwave back radiation from the water, J_c = conduction and convection, and J_e = evaporation and condensation are defined as

$$J_{an} = \frac{\sigma(T_{air} + 273)^4 \left(A + 0.031\sqrt{e_{air}}\right)(1 - R_L)}{10000} \tag{9}$$

$$J_{br} = \frac{\epsilon\sigma(T_1 + 273)^4}{10000} \tag{10}$$

$$J_c = \frac{c_1 f(U_w)(T_1 - T_{air})}{10000} \tag{11}$$

$$J_e = \frac{f(U_w)(e_{sat} - e_{air})}{10000} \tag{12}$$

where σ = Stefan-Boltzmann constant (11.7 x 10^{-8} cal cm^{-2} day^{-1} K^{-1}), A = atmospheric attenuation coefficient (0.5 to 0.7), e = vapor pressure (mmHg), R_L = reflection coefficient (≅ 0.3), ε = emissivity of the water (≅ 0.97), c_1 = Bowen's coefficient (≅ 0.47 mmHg C^{-1}), and U_w = wind speed (m s^{-1}) measured at a distance of 7 m above the water surface.

The dependence of heat transfer on wind velocity over the water surface is defined by $f(U_w)$; a definition for this relationship suggested by *TVA* [1972] is

$$U_w = U_{wz}\left(\frac{7}{z_w}\right)^{0.15} \quad (13)$$

$$f(U_w) = 19.0 + 0.95U_w^2 \quad (14)$$

where U_{wz} = wind speed (m s^{-1}) measured at a given distance of z_w (m) above the water surface.

The site or pool specific inputs for this model include: pool bathymetry (pool layer depth, z, volume, V, surface area, A_s, and surface area of the sediment, $A_{s,sed}$); influent water temperature, T_{in}; volumetric flow rate, Q_{in} and Q_{out}; and weather data (air temperature, T_{air}, wind speed, U_w, relative humidity, R_h, and incoming and reflected shortwave solar radiation, J_{sn}). Constants for this model include: specific heat, C_p, and emissivity of water, ε; atmospheric attenuation, A, and reflection coefficients, R_L; Stefan-Boltzmann constant, σ; Bowen's coefficient, c_1; thermal conductivity, K_{sed}, and diffusivity, α_{sed}, of the sediment; and temperature of the permafrost, T_{perm}. Parameters requiring calibration include the broad spectrum shortwave solar radiation attenuation coefficients, λ, and the vertical heat transfer coefficients, ν.

Because these pools have been found to be polymictic during the open water season, this phenomenon must be accounted for in the model formulation. Typical approaches applied within lake modeling were found to be inappropriate for well protected pools with very small surface areas (e.g., use of the Richardson number). Therefore, we incorporated a simple density gradient threshold at which pool layers

would mix. When the threshold is met, we use a simple mixing algorithm that applies a mass weighted approach:

$$T_{i,i+1} = \frac{T_i \rho_i V_i + T_{i+1} \rho_{i+1} V_{i+1}}{\rho_i V_i + \rho_{i+1} V_{i+1}} \quad (15)$$

Values for the density of water for each pool layer (ρ_i) were calculated within the model at every time step using the equations in the Appendix and also found in *Chapra and Martin* [2004].

Methodology

Site Description

This study applies this newly formulated temperature model to investigate the variability of pool temperature regimes in Imnavait Creek, a beaded stream located north of the Brooks Range on the north slope of Alaska in the Kuparuk River basin at 68.616°N latitude and 149.318°E longitude (Figure 3-2). Imnavait Creek flows north into Kuparuk River and then into the Arctic Ocean. Beaded streams, like Imnavait Creek, form when massive ground-ice deposits are exposed due to erosion by the stream [*McNamara et al.*, 1998].

This part of Alaska is wetland tundra and is completely underlain by several hundred meters of permafrost [*Osterkamp and Payne*, 1981], or permanently frozen ground. The top layer of soil, an organic peat layer 10 – 50 cm thick, overlies glacial till [*Hinzman et al.*, 1991]. The upper portion of the ground that experiences the freeze-thaw cycle, known as the active layer, typically reaches depths of approximately 25 – 40 cm in this area though depths of up to 100 cm have been recorded [*Hinzman et al.*, 1991].

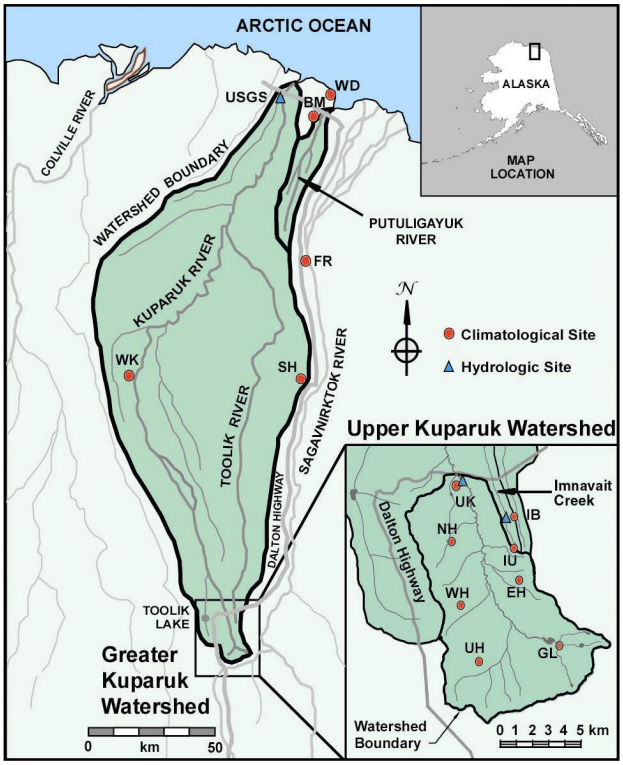

Figure 3-2. Greater Kuparuk Watershed showing the location of Imnavait Creek. (Courtesy of Doug Kane)

The area is effectively isolated from deep groundwater as the only subsurface storage and flow occur in the shallow active layer [*Edlund et al.,* 1990]. Although precipitation events and the associated surface and subsurface flow do occur during the open water summer season, the local hydrology is dominated by ablation of the snowpack [*Kane et al.*, 1989].

Data Collection

Several high spatial resolution datasets were collected within the pools, chutes and riparian area of Imnavait Creek in order to obtain detailed information on specific processes to support model formulation and population. This data was collected during a dry, low flow period from 1 – 6 July, 2010. We focused on this period because it is during this time that the limiting conditions of the temperature model assumptions hold

and stratification dynamics are such that they influence storage and export of water and other constituents of interest (e.g., nutrients). Additionally, this is the time of year when instream temperatures may be limiting habitat due to minimal precipitation and 24 hours of daylight.

This paper focuses on the datasets from a single pool in the creek having a surface area of approximately 3 m^2 and a depth of less than 1 meter. Given the simplifying assumptions of the model, this pool was selected for its apparent simplicity and the need to test basic instream processes without additional influences (e.g., lateral inflows due to water tracks or permafrost thaw). Once the dominant processes are determined and the model is developed for a single pool, we can then connect a series of pools to represent a stream reach.

Temperature Data

To understand the temperature dynamics within the water column, Onset® HOBO Water Temp Pro V2™ (Bourne, MA) temperature sensors were placed vertically within the pool (accuracy = 0.2 ºC over 0 to 50 ºC and resolution = 0.02 ºC at 25 ºC). Temperature in the water column was recorded every 5 minutes by 19 sensors at fixed depths approximately 3 cm a part in order to capture precise timing and vertical location of pool stratification. The sensors were wrapped in aluminum foil to avoid heating due to radiation penetration within the water [*Neilson et al*., 2010b]. Temperature in the water column was also verified several times throughout the study using a Fluke® 5610™ thermistor (American Fork, UT) (accuracy = 0.01 ºC and resolution = 0.0001 ºC over 0 to 100 ºC) by measuring water temperature at 1 cm increments. These measurements were

consistent with those recorded by the HOBOs verifying that the HOBO sensors were not significantly affected by solar heating.

Soil temperature vertical arrays were installed to establish boundary conditions for the riparian sediments. Onset® HOBO Water Temp Pro V2™ thermistor temperature sensors were used to record the temperature in the sediment every 5 minutes. The installation methods and depths used were similar to those described in *Neilson et al.* [2009]. The sensors for these sediment temperature arrays were placed in capped and perforated 1.5" PVC pipe at depths of at 3, 9, and 20 cm. The sensors were isolated vertically from each other so as to measure temperature at a specific depth. The intent of this configuration was to allow for lateral flow through the pipe, but prohibit vertical flow within the pipe. There were 4 sediment arrays buried around the pool for a total of 12 sensors.

Additional Data Types

Other data types were required in addition to temperature to document the ambient stream conditions. Weirs were installed at the inlet and outlet of the pool to facilitate measurement of volumetric flows. The low instream flow necessitated measurement using a simple bucket method where a 1 liter beaker was used to capture water flowing over the weirs. Air temperature and relative humidity measurements at 1, 3, and 10 meter heights were recorded hourly using Campbell Scientific® Model 207 (Logan, UT) temperature (accuracy = 0.4 ºC over -36 to 49 ºC) and humidity (accuracy = 5% over 12 to 100%) sensors from a meteorological station on the west-facing ridge of the basin approximately 1 kilometer upstream of the study site. An average value of the

measurements at the three heights for each sample increment was used as forcing data within the model. Wind speed was measured at approximately 40 cm above the water surface within the study reach using a Campbell Scientific® WindSonic™ Anemometer (Logan, UT) (accuracy = 2% of the reading over 0 to 60 m s^{-1}). Incoming shortwave solar radiation and water surface albedo were measured using two Hukseflux® LP02 (Logan, UT) pyranometers located just above the surface of a pool upstream of the study pool to ensure an undisturbed water surface. Shortwave solar radiation penetration through the water column was measured in 2009 to calculate an attenuation coefficient using methods similar to those found in *Neilson et al.* [2009; 2010a]. A detailed site survey including bathymetry was performed using a Trimble® GPS (Dayton, OH) system. From this high resolution geometric information, we were able to produce depth isopleths at 5 cm increments which were further interpolated within the model to calculate volumes (V_i) and surface areas ($A_{s,i}$). Thaw depths in and around the pools were measured using a graduated probe.

Model Population

In addition to providing specific information about heat fluxes between the pool and sediment layers, the field study provided information necessary to populate the temperature model. Vertical temperature profiles were created using data from the temperature sensors placed within the pool water column. These vertical profiles were then used to estimate the depths at which the temperature profile of the pool consistently changed. These depths represent the boundaries of the pool layers (z_i) within the model. With the depth of each pool layer established, the bathymetric data was interpolated

within the model to determine the volume (V_i), surface area of the layer-layer interface ($A_{s,i}$), and wetted sediment surface area ($A_{s,sed,i}$) of the pool layers. Once the geometry of the pool layers was established, the average observed temperatures of each layer were calculated using the associated sensors for use in model calibration and validation. Analysis of the detailed vertical water temperature array data also revealed information regarding diel mixing between layers occurring within the pool. This information was used to set the density gradient threshold for mixing within the model.

Average soil temperatures at depths of 3, 9, and 20 cm were calculated using all four vertical soil temperature arrays. These average soil temperatures were then used to fit a linear regression to represent a vertical temperature profile of the riparian sediments. The temperature of the sediments ($T_{sed,1}$ and $T_{sed,2}$ in eqs. 1 and 2) at the average depths corresponding to the top and middle pool layers were then established from this regression. Because the distance from the vertical soil temperature arrays to the pool edge was known ($z_{sed,1}$ and $z_{sed,2}$ in eqs. 1 and 2), these soil temperatures were then used as boundary conditions for the estimate of bed conduction between the riparian sediments and associated pool layers.

Depth of thaw beneath the pool ($z_{sed,3}$ in eq. 3) was based on a single measurement of sediment depth using a graduated probe at approximately the same time of year in 2009. Distance above the water surface at which wind speed was measured (z_w in eq. 13) was approximately 0.4 m. The value used for the inlet and outlet volumetric flow rates (Q_{in} and Q_{out} in eqs. 1 and 2) was an average of the values measured at the inlet weir over the first four days of the field study. Temperature of the permafrost (T_{perm} in eq. 6) was assumed to be 0 ºC.

Certain values used in the model were published values, either taken as a fixed constant or an estimated average. For example, the values for emissivity of water (ε), the atmospheric attenuation (A) and reflection coefficients (R_L), Stefan-Boltzmann constant (σ), and Bowen's coefficient (c_1) were taken from *Chapra* [1997]. The values for the thermal conductivity (K_{sed}) and diffusivity (α_{sed}) of the sediment were estimated as averages of those values found to be representative [*Chapra and Martin*, 2004; *Hinzman et al.,* 1991; *Kane et al.,* 1991].

Model Calibration

Model calibration was performed using the dataset from 1 – 3 July based on a sum root mean square error (RMSE) objective function. Individual RMSE values were calculated for all three pool layers which were then summed for each individual simulation. To determine the most appropriate combination of parameters that resulted in the smallest sum RMSE, ranges for the primary calibration parameters (shortwave solar radiation attenuation coefficients (λ) and vertical heat transfer coefficients (ν)) needed to be established. Ranges of these parameters were determined either from field data or based on a simple sensitivity analysis. To sample the parameter space, each parameter was incremented within its range and all unique combinations of parameters were established. Simulations were then run for each parameter combination and sum RMSE values were calculated. The most appropriate calibration parameter set was then chosen based on the lowest sum RMSE value.

Parameter ranges for the broad spectrum shortwave solar radiation attenuation coefficients were based on a field measurement in a 2009 study of approximately 9 m^{-1}.

However, the antecedent conditions in the 2010 study differed from those in 2009 resulting in variable water quality (e.g., DOC and TSS concentrations) and, therefore, different attenuation. Additionally, the attenuation within a pool is hypothesized to vary with depth due to stratification and the differences in water quality. With this information, the range set for the shortwave solar radiation attenuation coefficients was 9 – 20 m^{-1} and parameter combinations within model calibration were established based on 1 m^{-1} increments.

Published values for vertical heat transfer coefficients were found for large water bodies no shallower than depths of ~10 meters [e.g., *Chapra*, 1997]. Because no values were found for shallow, stratified water bodies with small surface areas, a first run calibration was performed using a large range for the vertical heat transfer coefficients of 0 – 1 m day^{-1} from which parameter combinations were established based on course increments of 0.1 m day^{-1}. After the initial calibration, this was refined to ranges equal to or less than 0.2 m day^{-1} at increments of 0.01 m day^{-1}. Validation of the model was based on comparison of model results from 4 – 6 July using the calibrated parameters.

Once the model was validated, characteristic times of the bottom pool layers, $\tau_{c,i}$, were calculated. For layers 2 and 3, the following relationship was used

$$\tau_{c,i} = \frac{\nu_{i-1,i} A_{s,i}}{V_i} \tag{16}$$

The average residence time for layer 1 was calculated as

$$\tau_1 = \frac{Q_{in}}{V_1} \tag{17}$$

Climate Change Scenarios

With the validated model we conducted simple climate change related scenarios to quantify the potential influence of these changes on instream temperatures and stratification patterns. According to several publications [e.g., *Chapman and Walsh*, 1993; *Serreze et al.*, 2000; *Wang and Key*, 2003], average temperatures at high latitudes have increased by up to 2 ºC over the last few decades and response of the Arctic to this continuing trend is predicted to become amplified. To estimate the potential effect of this change, the forcing data for air temperature (T_{air}) was changed by ±2 ºC. The second scenario simulates the potential impact of changes in depth of thaw due to climate change [*Hinzman et al.*, 1991] by changing the depth of the bottom sediment layer ($z_{sed,3}$) by ±20 cm.

Results

At the beginning of the field study when conditions were dry and flows were low, the pool was strongly stratified throughout the entire water column during the day while the upper portion would mix nightly (Figure 3-3). When precipitation occurred, solar radiation levels and air temperature were low and the pool would mix, sometimes completely as can be seen on 6 – 8 July. After 6 July, the increase in volumetric flow rate due to precipitation raised the water level in the pool significantly (by more than 20 cm) thereby changing the volume of the pool and its layers. Since this drastic change in pool volume violated the model formulation assumption of constant volume, our simulation period only spanned 1 – 6 July.

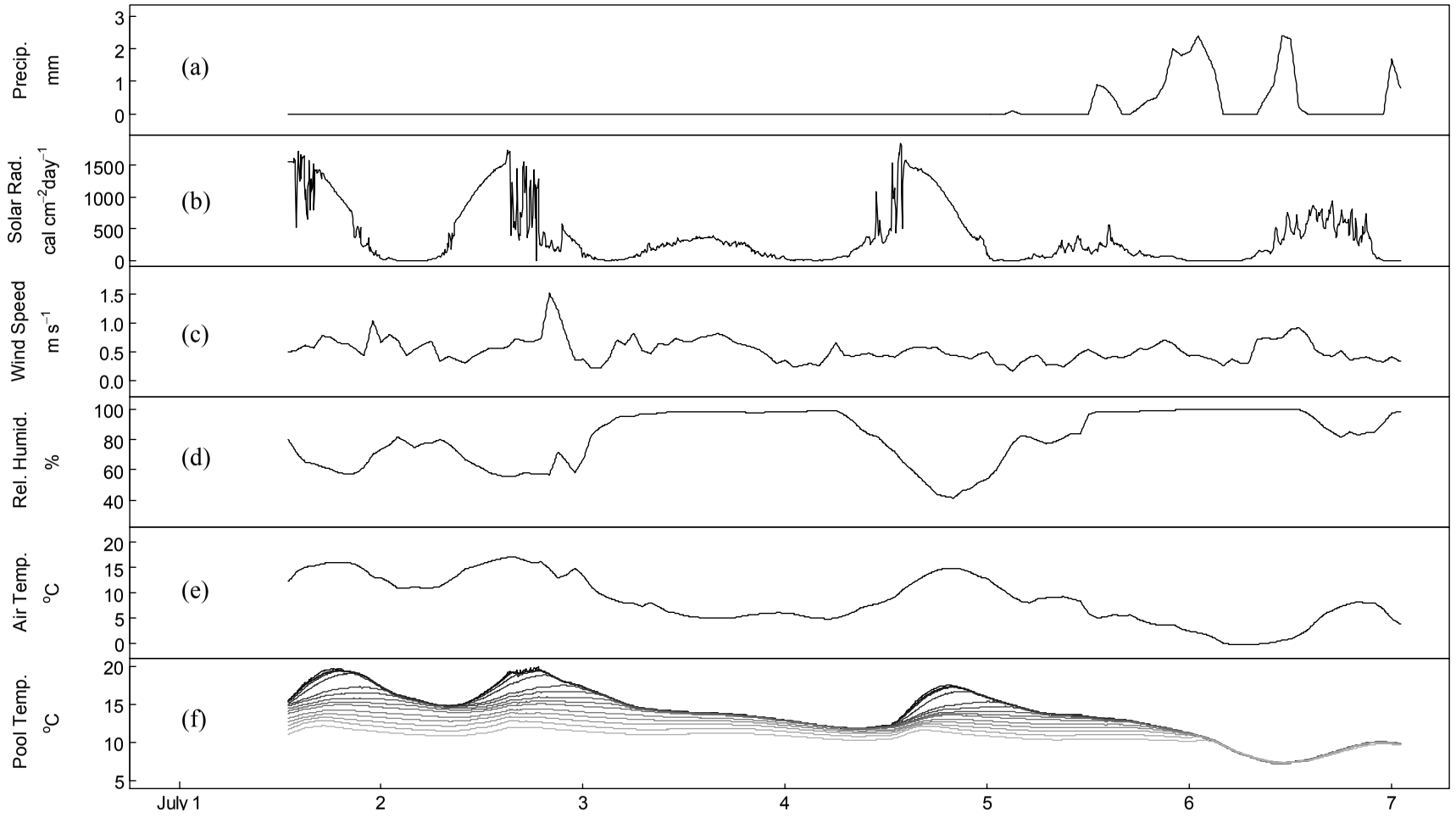

Figure 3-3. Time series of meteorological data collected on site and from a station on the west-facing ridge of the basin approximately 1 kilometer upstream of the study site (a-e) and vertical array temperatures in the pool (f). The sensors were placed every 3 cm within the water column. The darkest line represents the top sensor; subsequent lines become lighter with depth of each sensor.

Model Population

Figure 3-4 presents the temperature profiles of the pool created using the vertical water temperature array data. There are two obvious breaks in the series of profiles at depths of approximately 20 and 40 cm. These depths represent the boundaries imposed on the pool layers in the model (z_2 and z_3) thereby defining the volumes of all three completely mixed layers of the pool. Values for volume (V_i), surface area of the layer-layer interface ($A_{s,i}$), and wetted sediment surface area ($A_{s,sed,i}$) of the pool layers were calculated within the model by interpolating the bathymetric data based on the input values of the depth of the pool layers (Table 3-1).

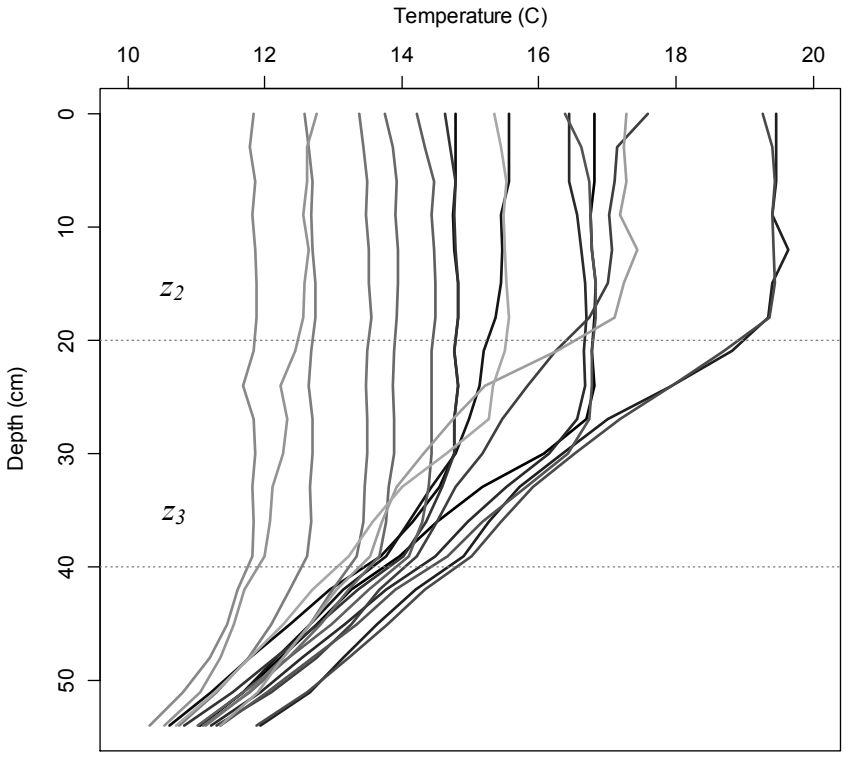

Figure 3-4. Vertical water temperature profiles of the pool at six hour increments throughout the study. The darkest line represents the earliest profile on 1 July and midnight; subsequent lines become lighter with the date and time of each profile.

Table 3-1. Values Used In Model Population Including Calculated/Interpolated Values, Constants, and Calibrated Parameters

Variable	Value	Units	Variable	Value	Units	Variable	Value	Units
z_1	0	m	$A_{s,1}$	10.294	m^2	$Q_{in,out}$	44.4	$m^3\ d^{-1}$
z_2	0.2	m	$A_{s,2}$	5.846	m^2	K_{sed}	$1.93x10^4$	cal d^{-1} m^{-1} $ºC^{-1}$
z_3	0.4	m	$A_{s,3}$	2.702	m^2	α_{sed}	0.025	$m^2\ d^{-1}$
$z_{sed,1,2}$	0.5	m	$A_{s,sed,1}$	5.228	m^2	C_p	1	cal g^{-1} $ºC^{-1}$
$z_{sed,3}$	0.55	m	$A_{s,sed,2}$	3.69	m^2	σ	$11.7x10^{-8}$	cal d^{-1} cm^{-2} K^{-1}
V_1	1.592	m^3	$A_{s,sed,3}$	3.018	m^2	A	0.6	-
V_2	0.836	m^3	$v_{1,2}$	0.14	m d^{-1}	R_L	0.3	-
V_3	0.278	m^3	$v_{2,3}$	0.11	m d^{-1}	ε	0.97	-
$T_{sed,1}$	10	ºC	λ_1	14	m^{-1}	c_1	0.47	mmHg $ºC^{-1}$
$T_{sed,2}$	7	ºC	λ_2	12	m^{-1}	z_w	0.4	m
T_{perm}	0	ºC				$\Delta\rho$	20	$g\ m^{-3}$

The temperature profile of the riparian sediments created from the vertical sediment temperature array data provided a way to estimate temperatures of the top ($T_{sed,1}$ = 10 ºC) and middle ($T_{sed,2}$ = 7 ºC) sediments. The approximate distance of the four vertical sediment temperature arrays from the pool edge ($z_{sed,1,2}$) was set in the field at 0.5 m. The volumetric flow rate of the stream (Q) was calculated as the average of measured rates from the field. The value for specific heat of water (C_p) and temperature of the permafrost (T_{perm}) were assumed. Based on the diel mixing occurring in the top layers of the pool, it was found that when the difference in density between pool layers ($\Delta\rho$) became less than 0.00002 g cm^{-3}, mixing occurred between the appropriate layers (Table 3-1).

Values reported in various publications for the thermal conductivity (K_{sed}) and diffusivity (α_{sed}) for the sediments within the Imnavait Creek watershed are presented in

Table 3-2. The average values ($1.93x10^4$ cal day^{-1} m^{-1} $ºC^{-1}$ and 0.025 m^2 day^{-1} for the thermal conductivity (K_{sed}) and diffusivity (α_{sed}), respectively) were used in the modeling effort.

Model Calibration and Validation

The parameter set established in model calibration was based on the lowest sum RMSE of 0.92 ℃, resulting in parameter values of 0.14 and 0.11 m day^{-1} for the vertical heat transfer coefficients ($\nu_{1,2}$ and $\nu_{2,3}$) and 14 and 12 m^{-1} for the shortwave solar radiation attenuation coefficients (λ_1 and λ_2) (Figure 3-5). In addition, RMSE values for the middle and bottom layer from the calibration dataset are within the accuracy of the temperature sensors used to generate the observational datasets (Figure 3-5). The residence times calculated for the pool layers based on the calibration parameter set and

Table 3-2. Published Values for Thermal Conductivity and Diffusivity of Sediment Unpublished Values Are Denoted With an (*)

Publication	α_{sed} m^2 d^{-1}	K_{sed} cal d^{-1} m^{-1} C^{-1} ($x10^4$)	Location
Kane et al.	*	2.27	within upper 0.6 m near Toolik Lake
[1991]	*	2.68	beyond the upper 0.6 m near Toolik Lake
Hinzman et at.	*	1.96	saturated organic
[1991]	*	1.14	mineral soils
Chapra and	0.0104	0.778	wet peat
Martin	0.0173	0.950	gelatinous lake sediments
[2004]	0.0518	3.72	loam (75% saturated)

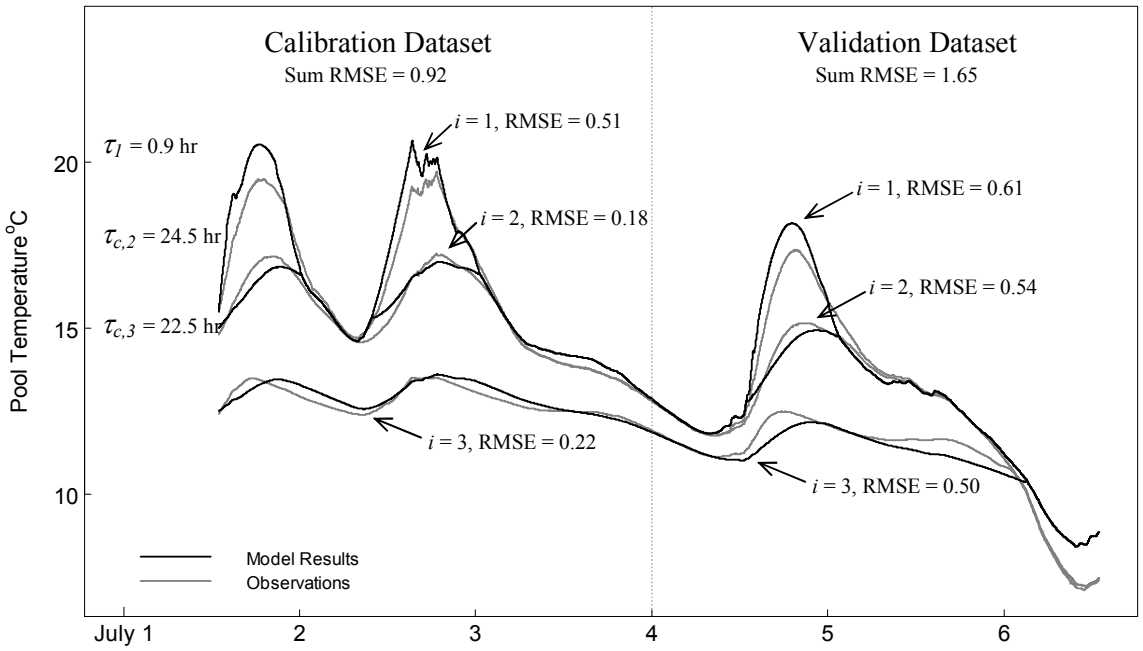

Figure 3-5. Model results using the calibrated parameter set based on the lowest sum RMSE and average temperature measurements from sensors corresponding to the model layers. Where *i*=1 is layer 1, *i*=2 is layer 2, and *i*=3 is layer 3.

using equations (17) and (18) are 0.9 h, 24.5 h, and 22.5 h for the top, middle and bottom layers, respectively.

With the model populated and calibrated, it was then validated against field observation data from 4 – 6 July (Figure 3-5). As can be seen in the calibration dataset from 1 – 3 July, the estimated temperatures of all three layers are within a degree of observed temperatures. Also, timing of the diel cycle and mixing of the layers are near observed timing. The same can be said for the validation dataset from 4 – 6 July other than the overestimation on 6 July for all three pool layers. However, 6 July marks the beginning of the transition point at which consistent precipitation began and the model assumptions no longer hold true. Overall for both calibration and validation datasets, the

upper layer overestimates the peaks, the middle layer slightly underestimates the peaks, the timing of the diel cycle of the lower layer is slightly off, and the timing of mixing of the layers is somewhat delayed at times. However, given the simple treatment of complex hydrodynamics within the system, the closeness of fit suggests that the dominant heat transfer mechanisms are represented within the model.

The various heat fluxes calculated in the model for each pool layer are vastly different (Figure 3-6). Although each layer is driven by a different heat flux throughout the day (Figures 3-6 and 3-7), all fluxes within each layer account for more than 10% of the total heat flux per layer. The exception to this is the first layer, which is overwhelmingly driven by the atmospheric and advective fluxes. Depending on the time of day, the second layer is driven primarily by either the atmospheric flux or exchange with the bottom layer. The bottom layer is largely driven by the sediment flux.

The atmospheric fluxes were further broken down (Figure 3-8) to quantify the individual influence within each layer. The shortwave solar radiation for each pool layer (Figure 3-8a) provides a glimpse on the influence of attenuation of radiation through the water column. The atmospheric heat fluxes for the top pool layer (Figure 3-8b) illustrate the relative importance of each of these terms (J_{an}, J_{sn}, J_{br}, J_e, and J_c) within the total surface flux (J_{atm}) and, therefore, on the energy budget for the top layer.

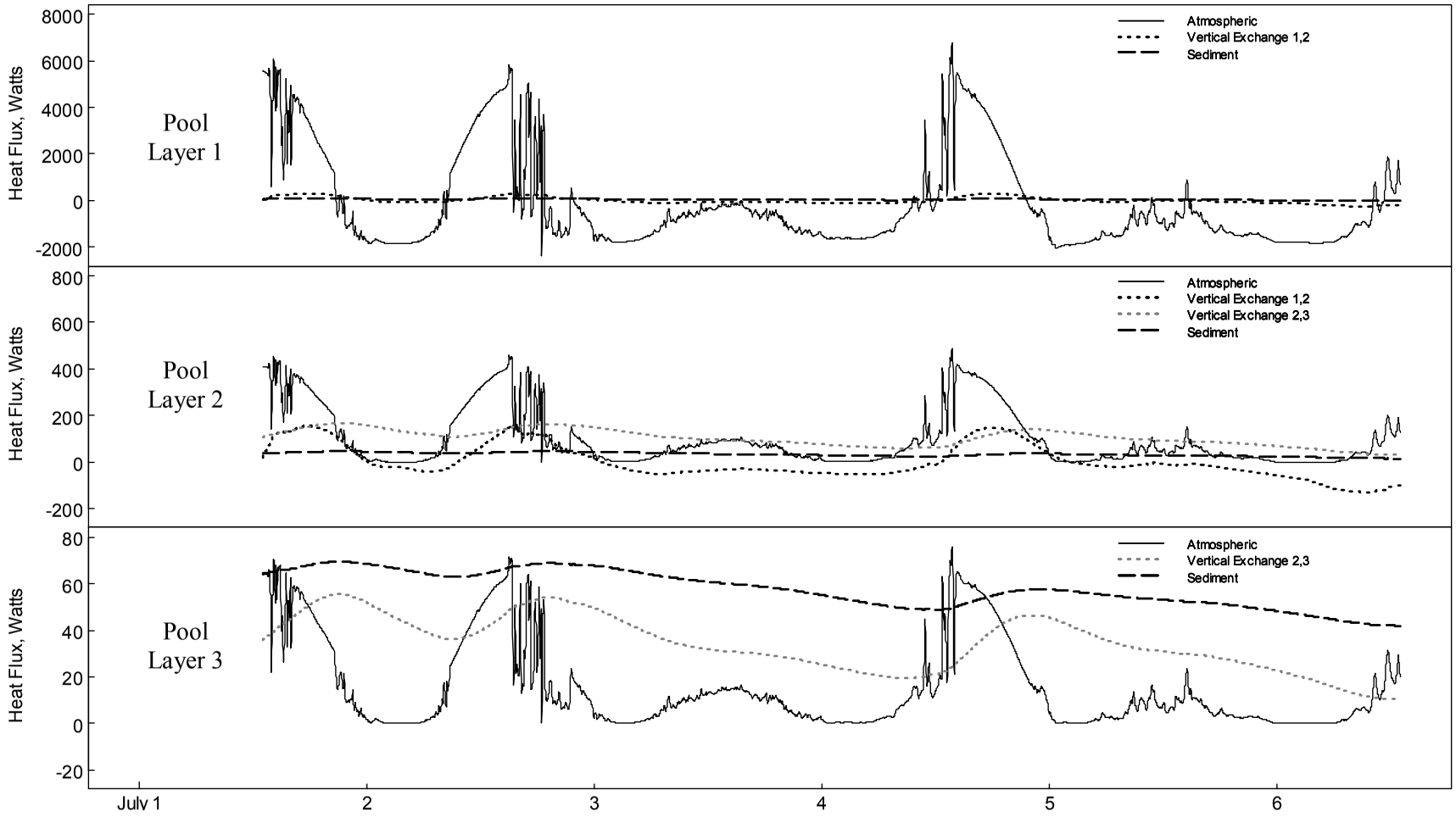

Figure 3-6. Heat fluxes associated with each pool layer. Note that the y-axis differs for each layer by an order of magnitude.

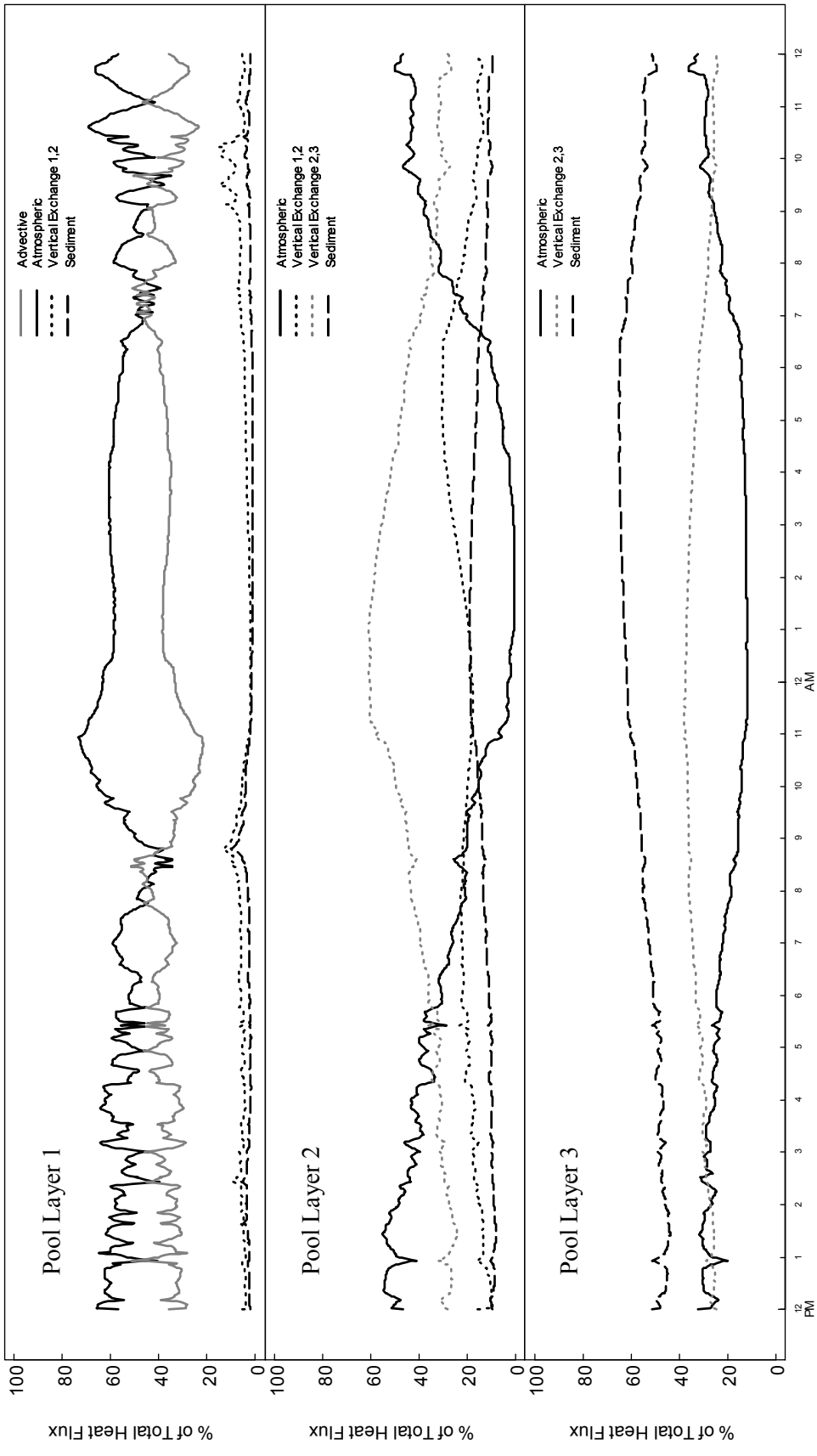

Figure 3-7. Average heat fluxes associated with each pool layer as a percent contribution to the total heat flux over a 24-hour period. Advective heat flux is the difference between inflow and outflow.

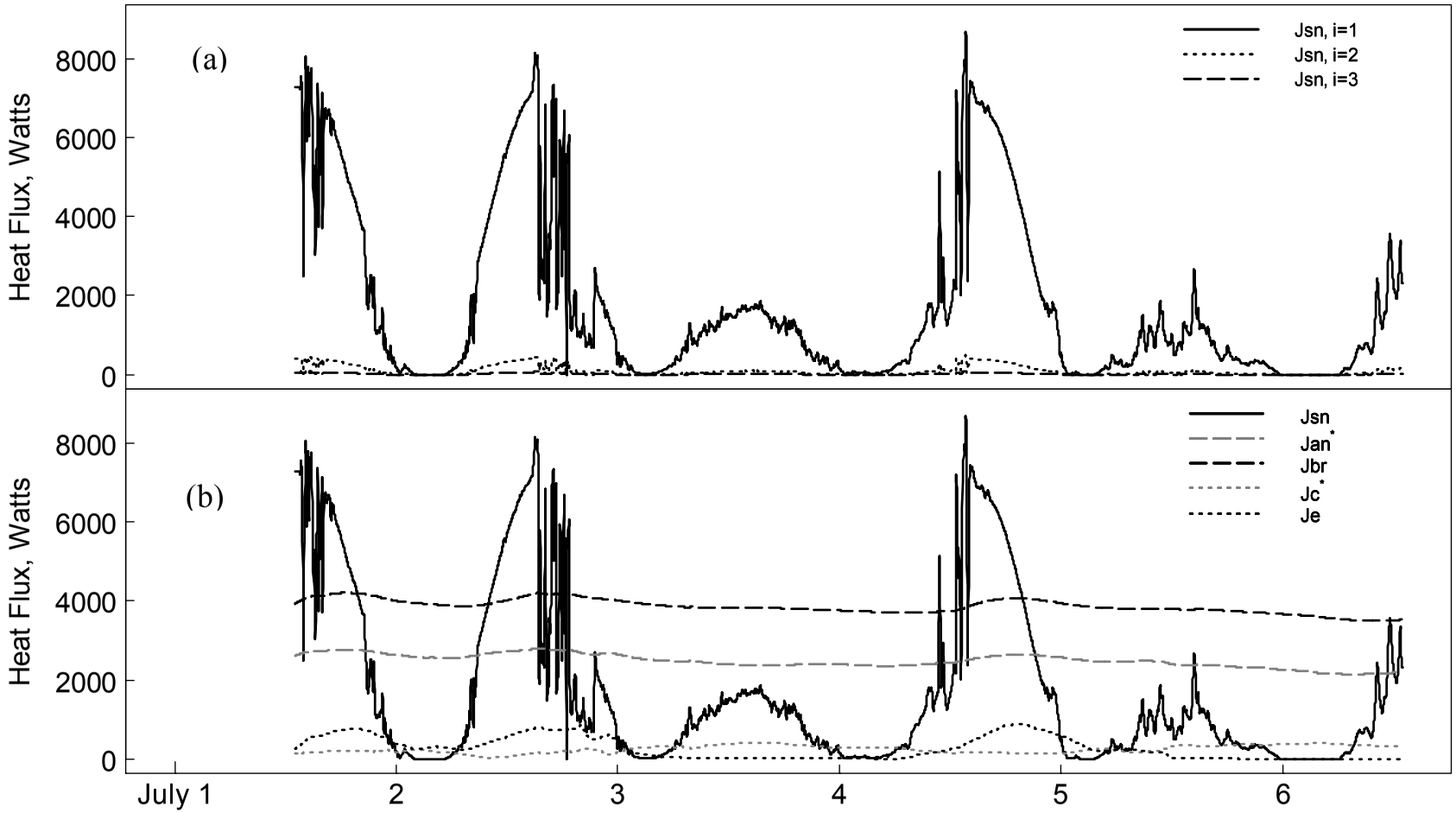

Figure 3-8. Shortwave solar radiation (Jsn) in each pool layer (a) and each individual component of atmospheric fluxes in pool layer 1 (b). The difference in amount of J_{sn} absorbed by each layer is attributable to the attenuation of the radiation through the water column (in plot a). Fluxes with * are those affected by air temperature (in plot b).

Climate Change Scenarios

The first climate change scenario accounted for changes in air temperature by ±2 ºC (Figure 3-9). The second scenario simulated changes in depth of thaw by changing the depth of the bottom sediment by ±20 cm, which is a potential impact of changing air temperatures. This scenario resulted in drastic changes in temperatures in the water column, particularly the lower layers that have greater contact area with the sediments (Figure 3-10). The resulting changes in pool layer temperatures affect both the pattern and timing of mixing of layers, which subsequently affects the water residence time of each layers.

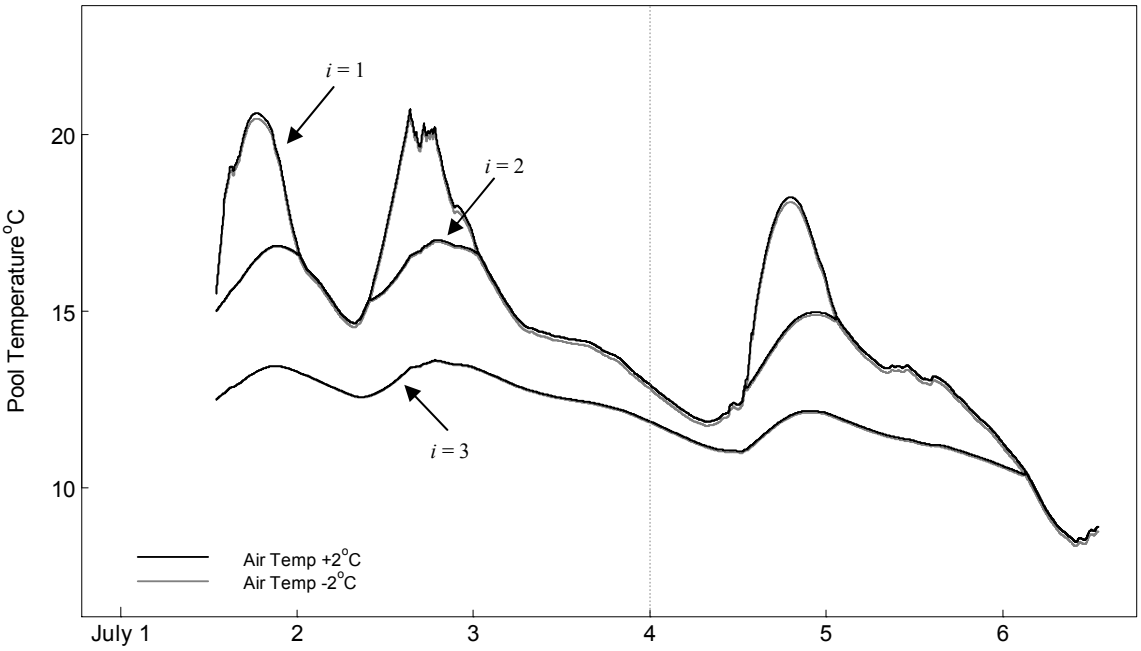

Figure 3-9. Climate change simulation results for changing air temperature by ±2ºC. Where *i*=1 is layer 1, *i*=2 is layer 2, and *i*=3 is layer 3.

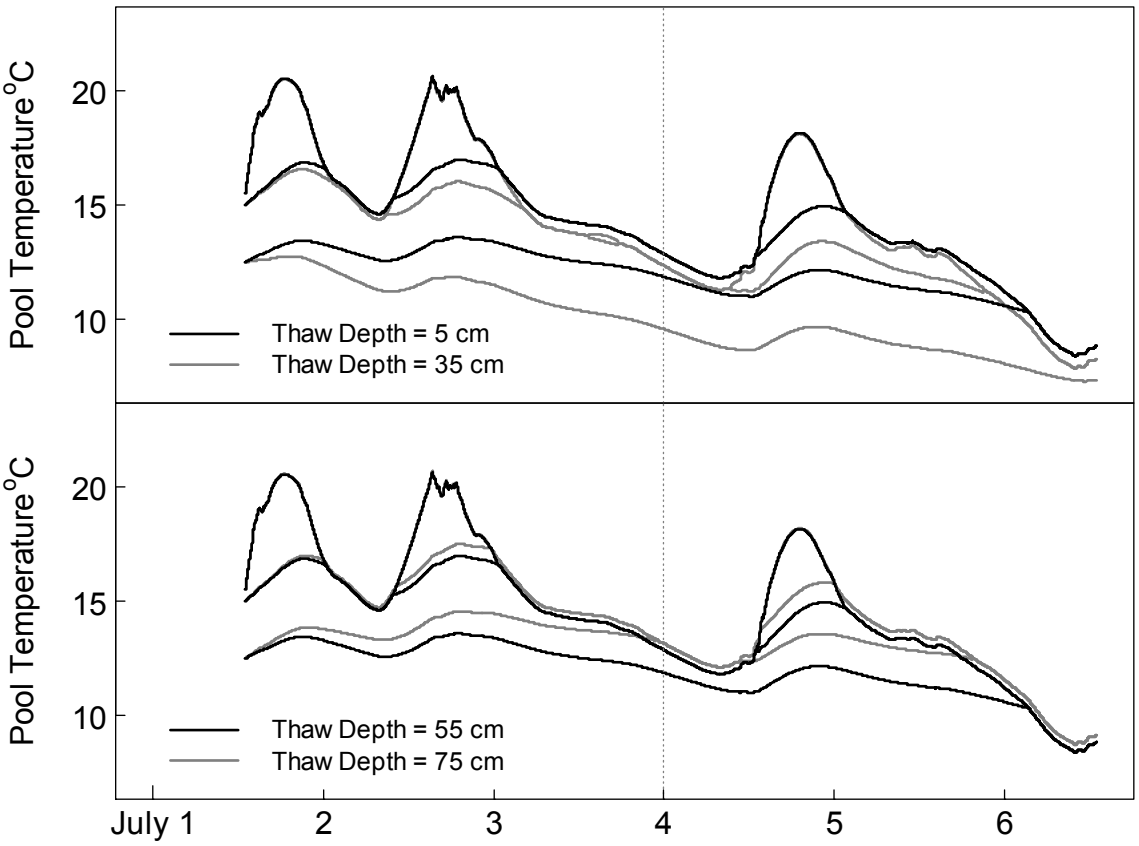

Figure 3-10. Climate change simulation results for changing depth of thaw by ±20 cm. Where *i*=1 is layer 1, *i*=2 is layer 2, and *i*=3 is layer 3. The 55 cm depth is associated with the original calibration.

Discussion

Given the thermal stratification and diel mixing observed in field data (Figures 3-3f and 3-4), the pools in this stream do not follow a distribution of heat fluxes typical of stream/lake systems [*Caissie*, 2006; *Johnson*, 2004; *Neilson et al.,* 2009; *Webb et al.,* 2008]. It was therefore necessary to develop a site specific modeling approach in order to incorporate the heat flux terms required of the small size and unique characteristics of beaded streams (e.g., high instream temperatures, thermal stratification, and presence of

permafrost). The result was a distribution of heat fluxes that differ significantly per layer (Figure 3-6). For example, the magnitude of absorbed radiation within each layer varies (Figure 3-8a), however, this heat flux within each layer is considerable (Figure 3-6). While photosynthetic active radiation (PAR) attenuation through the water column is important when modeling the photic zones of lakes [*Dodds*, 2002], the impact of shortwave radiation penetration is rarely accounted for in the heat budgets (e.g., CEQUAL-R1 [*Environmental Laboratories*, 1990], and LAKE2K [*Chapra and Martin*, 2004]) because it is reasonable to assume all radiation is absorbed within the top layer of a deep lake. Similarly, shortwave radiation penetration is rarely accounted for within stream models (with the one known exception of HeatSource [*Boyd and Kasper*, 2004]). Within this application, we found that excluding shortwave radiation attenuation in the model formulation would have resulted in all radiation being absorbed in the top layer and, therefore, too high of temperatures in that upper layer. Additionally, temperatures within the lower layers would have been underestimated. Another heat flux that influences the lower layers is bed conduction, which is rarely influential in modeling temperatures within lakes or large rivers (e.g., CEQUAL-R1 [*Environmental Laboratories*, 1990], LAKE2K [*Chapra and Martin*, 2004], QUAL2E [*Brown and Barnwell*, 1987], and SNTEMP [*Theurer et al.*, 1984]). This emphasizes the importance of collecting process specific data to support model conceptualization.

Through use of these data in model conceptualization and development, we identified a number of datasets that were imperative to accurate temperature predictions. First, we found that the model is sensitive to the volumes (V) and surface areas (A_s) of the pool and sediment layers. Therefore, it is important to obtain high resolution bathymetry

and temperatures in the water column in order to determine these values. Also, by collecting site specific broad spectrum shortwave radiation attenuation measurements at a fine vertical resolution, layer specific attenuation coefficients can be determined and parameter uncertainty can be reduced.

Final model calibration parameters were determined using the lowest sum RMSE as our optimal objective function. However, several parameter sets resulting in similar model fits could have been used. The parameter ranges representing sum RMSE values less than 1 ºC were: 0.11 – 0.15 m d^{-1}, 0.09 – 0.13 m d^{-1}, 14 – 15 m^{-1}, and 11 – 13 m^{-1} for the vertical heat transfer ($\nu_{1,2}$ and $\nu_{2,3}$) and broad spectrum shortwave radiation attenuation coefficients (λ_1 and λ_2), respectively. These relatively small ranges suggest that the parameter uncertainty is acceptable within this application.

The first model simulation scenario represented climate change using changes in air temperature (T_{air}) based on recent meteorological trends found in the Arctic (i.e., seasonal increases in air temperature [*Chapman and Walsh*, 1993; *Serreze et al.*, 2000; *Wang and Key*, 2003]). The results of these simulations show that there is little direct impact on instream temperatures with the forced changes (Figure 3-9). Based on the model formulation, the only equations including air temperature are for calculating the net atmospheric longwave radiation (J_{an} in eq. 9) and the conduction and convection (J_c in eq. 11). Similarly, increases in wind speed [*Hinzman and Kane*, 1992] would only influence conduction and convection (J_c in eq. 11) and evaporation and condensation (J_e in eq. 12). In both cases, the magnitudes of the terms affected by air temperature and wind speed (J_{an}, J_c, and J_e) relative to incoming net solar shortwave radiation (J_{sn}) are small and, therefore, will likely have little impact on the total surface flux (J_{atm}) of the top

pool layer. Drastic changes in wind speed may, however, result in different mixing patterns due to shear stress at the water surface.

Simulating climate change by simply changing the air temperature or increasing wind speed does not represent the entirety of changes that would occur within the watershed due to shifting weather patterns (e.g., higher instream flows [*Mangnuson et al.*, 2000], more runoff due to snowmelt [*Sturm et al.*, 2005], changes in depth of thaw [*Hinzman et al.*, 1991], etc.). Therefore, the second scenario represented a more holistic influence on the watershed due to changing climate conditions through changes in depth of thaw ($z_{sed,3}$). The depth of thaw only directly influences the sediment flux in the bottom pool layer (eq. 3), however, it is the dominant heat flux for that layer (Figures 3-6 and 3-7). The results of these simulations show that changing the depth of thaw heavily influences overall instream temperatures primarily due to changes in temperature of the bottom layer that influences stratification and mixing patterns. The net result of these changes would be a shift in the timing of water export, which impacts the fate and transport of heat, nutrients, and other constituents of interest.

As shown in Chapter 2, lateral inflow from the active layer due to precipitation can also change stratification and mixing patterns. Pool temperatures can be influenced by lateral inflow from storage in the active layer, which is impacted by the depth of thaw [*McNamara et al.*, 1997]. We also anticipate that changes in precipitation patterns [*Hinzman and Kane*, 1992] will affect storage in the active layer and therefore drastically influence lateral inflows. Both of which can further impact temperature and export dynamics. There was shown to be little or slowed movement of water into and out of the lower layers of the pools in this stream when stratified. This slowed movement and

exchange between layers represents longer storage and residence times. The marked difference in calculated residence times of the top and lower layers of the pool in this study support this finding (Figure 3-5).

Dynamics of storage and export of water highly influence the movement of heat and mass through watersheds [*McNamara et al.,* 1998]. This is significant because it impacts the movement of nutrients, which are limiting in most Arctic systems [*Brooks and Williams,* 1999; *Chapin et al.,* 1980; *Dowding et al.*, 1981; *Kling,* 1995; *Satoru et al.*, 2006]. Changes in storage and residence times can have basin wide effects, from impacting instream temperatures during critical times to changes in chemical and biological processes downstream. These effects suggest that Imnavait Basin and similar beaded Arctic watersheds will experience delayed export of water and other constituents compared to other stream types within the Arctic.

Conclusion

The purpose of our study was to investigate instream heat fate and transport in a beaded Arctic stream through the development of a temperature model, which includes advective, surface, and bed conduction fluxes, simplified vertical exchange between stratified layers, and attenuation of shortwave radiation through the water column. The model provides a simplified representation of temperature stratification and mixing patterns under steady low flow conditions within a small pool in a beaded stream located on the North Slope of Alaska. Collection of several high resolution datasets was necessary to support model conceptualization and development. Given the thermal stratification and diel mixing observed in these data, we concluded that the pools in this

stream do not follow a distribution of heat fluxes typical of stream/lake systems. Because of this and due to the small size and unique characteristics of the stream (e.g., high instream temperatures, thermal stratification, and presence of permafrost), heat flux terms that would otherwise be ignored were required in the energy balance for model formulation. This relatively simple approach produced model results that capture the temperature responses observed within our calibration and validation datasets. We found that key data within this modeling effort include attenuation of shortwave radiation through the water column, high resolution temperatures in the water column, and high resolution bathymetry.

The results from our climate change scenarios show that air temperature has little effect on instream temperatures in beaded Arctic streams. However, changes in depth of thaw heavily impact instream temperatures, particularly in the lower pool layers that have greater contact area with the sediments. The changes in temperature of these lower layers affect the stratification and mixing patterns, which influence export of water and therefore fate and transport of heat, nutrients, and other constituents of interest.

CHAPTER 4

CONCLUSION

The purpose of this study was to investigate the fate and transport of mass and heat within a beaded Arctic stream. This was investigated through identification of water storage types and patterns by tracing water flow paths in and around the study reach. Using primarily synoptic measurements of specific conductivity and temperature profiles, we gained insight into the patterns of wetting and drying of the riparian sediments and stratification of the pools during dry to saturated conditions. Heat fate and transport was further investigated through the development of a temperature model, which includes advective, surface, and bed conduction fluxes, simplified vertical exchange between stratified layers, and attenuation of shortwave radiation through the water column of a single pool within the beaded stream.

As expected, the hydrologic connectivity of the hillslope to the riparian zone within this beaded Arctic watershed is both direct, through water tracks and runoff, and indirect, through diffuse lateral flow, and results in riparian storage of hillslope water. However, we found that riparian and hillslope storage can subsequently influence in-pool storage through subsurface lateral inputs. Conversely, when unsaturated, the available storage in the riparian zone can be influenced by lateral exchange of in-pool water when instream water levels increase.

Dry conditions with low flows facilitated greater in-pool storage and increased water residence times. This is primarily due to strong thermal stratification which produced large stores of cooler water with long residence times in the bottom layers of

the pools. However, even under high flow conditions, stratification was still observed in a pool influenced by cold lateral inputs. In the earlier portion of the thaw season, this water has the potential to be nutrient rich as the bulk of it is most likely from spring melt. Wet conditions with high flows resulted in complete or nearly complete mixing of the pools, which resulted in large volumes of instream waters flushing the long-term in-pool storage.

The temperature model developed within this thesis provides a simplified representation of the temperature stratification and mixing patterns observed under steady low flow conditions. Collection of several high resolution datasets was necessary to support model conceptualization and development. Given the thermal stratification and diel mixing observed in the instream temperatures, we concluded that the pools in this stream do not follow a distribution of heat fluxes typical of stream/lake systems. Because of this and due to the small size and unique characteristics of the stream (e.g., high instream temperatures, thermal stratification, and presence of permafrost), heat flux terms that would otherwise be ignored were required in the energy balance for model formulation. This relatively simple approach produced model results that capture the temperature responses observed within our calibration and validation datasets. We found that key data associated with this modeling effort include attenuation of shortwave radiation through the water column, high resolution temperatures in the water column, and high resolution bathymetry.

The results from the climate change scenarios show that air temperature and wind speed have little effect on instream temperatures in beaded Arctic streams. However, changes in depth of thaw heavily impact instream temperatures, particularly in the lower

pool layers that have greater contact area with the sediments. The changes in temperature of these lower layers affect the stratification and mixing patterns, which influence export of water and therefore fate and transport of heat, nutrients, and other constituents of interest.

This study has shown that the hydrology of Arctic watersheds with beaded streams is complex and quite dynamic. Overall, we found that the extent of water storage and residence times within these beaded systems are highly variable and greatly influence the timing and patterns of thermal stratification and mixing patterns and, therefore, influence water and material export dynamics. These dynamics are important due to the implications on downstream processes including impacts on ecology, fisheries, local subsistence residents, and nutrient export to the Arctic Ocean.

CHAPTER 5

ENGINEERING SIGNIFICANCE

This research presents advances in the fields of Environmental and Water Resources Engineering by providing insight into processes involving the fate and transport of heat and mass in beaded Arctic streams. This was accomplished through analysis of observational data and development of an instream temperature model. Due to the sensitivity of low energy environments and cold region processes [*Rouse et al.*, 1997], the effects of changing climate are of particular interest in the Arctic. However, beaded Arctic streams are among the least studied [*Oswood et al.*, 1989] and, therefore, our abilities to predict the impacts of climate change on these systems have been limited.

Observational data collected in support of model conceptualization and development offered an unexpected glimpse into the unique water storage and export patterns in beaded Arctic streams. Using temperature and various other data, we were able to document various types of storage within the pools, banks, and other marshy areas within the riparian zone, including subsurface flow paths that connect the pools. In doing so, we were able to capture patterns of stratification and mixing within the pools during a critical meteorological period transitioning from dry to wet conditions. It was found that these patterns influence water storage within the pool, which subsequently influences export of heat and mass, including constituents of interest.

The temperature model developed within this thesis provides a simplified representation of the observed stratification and mixing patterns under dry, low flow conditions within a small pool in the stream. To better understand potential impacts on

these systems due to climate change, various scenarios were simulated using the newly developed temperature model. Through these scenarios, we found that potential increases in thaw depths due to climate change can shift stratification and mixing patterns and, therefore, influence nutrient export dynamics. These advances are important due to the implications on downstream processes including impacts on ecology, fisheries, local subsistence residents, and nutrient export to the Arctic Ocean.

In addition, the observations made within this thesis based on both the field data and model results provide foundational information that will guide future hydrologic research in beaded Arctic watersheds. Further investigations should include: interactions between the hillslope, riparian, and instream zones; hillslope and riparian zone connectivity; exchange between the riparian zone and stream; and pool storage due to stratification.

CHAPTER 6

RECOMMENDATIONS FOR FUTURE RESEARCH

1) **Attenuation**: Higher resolution of attenuation measurements. The data in this study did not support accurate estimation of attenuation coefficients for each pool layer. Ideally, these values would have been estimated based on measurements taken at a fine vertical resolution while ensuring minimal mixing of the layers, thereby reducing the number of and uncertainty in the calibration parameters.

2) **Thaw Depth**: Higher density, both spatially and temporally, of thaw depth measurements under the pool. This study used a single measurement to represent the active layer over time and space. However, it was found that thaw depth is an important and sensitive model parameter warranting more attention during data collection. Additionally, collecting a time series of thaw depths would allow for inclusion of a more accurate representation of dynamic processes involving the thaw depth active layer interface in model formulation. Collection of this additional data would involve leaving temp sensors in place throughout a full freeze thaw cycle.

3) **Flow**: Broader range of flow conditions. Develop a stage discharge relationship in order to obtain flow time series data using data from a pressure transmitter along with the weirs. These data would allow for simulation of higher flow periods, thereby allowing precipitation and transition periods to be incorporate into the model formulation.

4) **Water and Side Track Flows**: Collect flow data for lateral inflow sources. Use weirs or other methods in the water and side tracks in order collect flow volumes. This would allow for seepage and/or other lateral inflows to be accounted for in the model formulation.

REFERENCES

Bense, V. F., and H. Kooi (2004), Temporal and spatial variations of shallow subsurface temperature as a record of lateral variations in groundwater flow, *J. of Geophysical Res., 109,* B04103, doi:10.1029/2003JB002782.

Boyd, M., and B. Kasper (2004), Analytical methods for dynamic open channel heat and mass transfer methodology for the heat source model version 7.0, 204 pp., Carollo Engineers.

Brooks, P. D., and M. W. Williams (1999), Snowpack controls on nitrogen cycling and export in seasonally snow-covered catchments, *Hydrol. Processes, 13,* 2177–2190.

Brown, G.W. (1969), Predicting temperatures of small streams, *Water Resour. Res., 5,* 68-75.

Brown, L.C., and T. O. Barnwell (1987), The enhanced stream water quality model QUAL2E and QUAL2E-UNCAS: documentation and user manual, United States Environmental Protection Agency, Athens, GA.

Caissie, D. (2006), The thermal regime of rivers: a review, *Freshwater Bio., 51,* 1389-1406.

Chapin, F. S. I., P. C. Miller, W. D. Billings, and P. I. Coyne (1980), Carbon and nutrient budgets and their control in coastal tundra, in *An Arctic Ecosystem: The Coastal Tundra at Barrow*, edited by J. Brown, P. C. Miller, L. L. Tieszen, and F. L. Bunnell, pp. 458–482, Dowden, Hutchinson & Ross, Stroudsburg, Penn.

Chapman, W.L., and J. E. Walsh (1993), Recent variations of sea ice and air temperatures in high latitudes, *Bull. Am. Meteorol. Soc., 74,* 33-47.

Chapra, S., and J. Martin (2004), LAKE2K: A modeling framework for simulating lake water quality (Version 1.2). (BETA TEST VERSION), Civil and Environmental Engineering Dept., Tufts University, Medford, Mass.

Chapra, S.C. (1997), *Surface Water Quality Modeling*, 844 pp., McGraw-Hill, Boston, Mass.

Chapra, S. C., and R. P. Canale (2006), *Numerical Methods for Engineers*, 634 pp., McGraw-Hill, New York.

Cirmo, P.C., and J. J. McDonnell (1997), Linking the hydrologic and biogeochemical controls of nitrogen transport in near-stream zones of temperate-forested catchments - a review, *J. of Hydrol., 199,* 88-120.

Dodds, W. K. (2002), *Freshwater Ecology Concepts and Environmental Applications,* Academic Press, San Diego, Calif.

Dowding, P., F. S. I. Chapin, F. E. Wielgolaski, and P. Kilfeather (1981), Nutrients in tundra ecosystems, in *Tundra Ecosystems, A Comparative Analysis*, edited by L. C. Bliss, O. W. Heal, J. J. Moore, pp. 647–683, Cambridge University Press, Cambridge.

Edlund, S.A., M.-K.Woo, and K. L. Young (1990), Climate, hydrology and vegetation patterns. Hot Weather Creek, Ellesmere Island, Arctic Canada. *Nordic Hydrol., 21,* 273–286.

Edwardson, K.J., W. B. Bowden, C. Dahm, and J. Morrice (2003), The hydraulic characteristics and geochemistry of hyporheic and parafluvial zones in Arctic tundra streams, north slope, Alaska, *Advances in Water Resour., 26,* 907-923.

Environmental Laboratories (1990), *CE-QUAL-R1: A dynamic one-dimensional (longitudinal) water quality model for streams User's manual*, U. S. Army Corps of Engineers, Waterways Experiment Station, Vicksburg, Miss.

Haggerty, R., S. M. Wondzell, and M. A. Johnson (2002), Power-law residence time distribution in the hyporheic zone of a 2nd-order mountain stream, *Geophysical Res. Letters, 29*(13), 1640, doi:10.1029/2002GL014743.

Hinzman, L.D., and D. L. Kane (1992). Potential response of an Arctic watershed during a period of global warming. *J. of Geophysical Res., 97,* 2811-2820.

Hinzman, L.D., D. L. Kane, R. E. Gieck, and K. R. Everett (1991), Hydrologic and thermal properties of the active layer in the Alaskan Arctic, *Cold Regions Sci. and Technol., 19,* 95-110.

Inamdar, S., J. Rupp, and M. Mitchell (2009), Groundwater flushing of solutes at wetland and hillslope positions during storm events in a small glaciated catchment in western New York USA. *Hydrol. Processes, 23,* 1912-1926.

Irons, J.G. III, and M. W. Oswood (1992), Seasonal temperature patterns in an Arctic and two subarctic Alaskan headwater streams, *Hydrobiologia, 237,* 147-157.

Johnson, S. L. (2004), Factors influencing stream temperatures in small streams: substrate effects and a shading experiment, *Canadian J. of Fisheries and Aquatic Sciences, 61,* 913–923.

Kane, D.L., L.D. Hinzman, C. S. Benson, and K. R. Everett (1989), Hydrology of Imnavait Creek, an Arctic watershed, *Holarctic Ecology, 12,* 262-269.

Kane, D.L., L. D. Hinzman, J. P. McNamara, Z. Zhang, and C. S. Benson (2000), An overview of a nested watershed study in Arctic Alaska, *Nordic Hydrol., 31,* 245-266.

Kane, D. L, L. D. Hinzman, and J. P. Zarling (1991), Thermal response of the active layer to climatic warming in a permafrost environment, *Cold Regions Sci. and Technol., 19,* 111-122.

Kling, G.W. (1995), Land-water linkages: the influence of terrestrial diversity on aquatic systems, in *The Role of Biodiversity in Arctic and Alpine Tundra Ecosystems*, edited by Chapin F.S. and C. Korner, pp. 297-310, Springer, Berlin.

Mangnuson, J.J., D. M. Robertson, B. J. Benson, R. H. Wynne, D. M. Livingstone, T. Arai, R. A. Assel, R. G. Barry, V. Card, E. Kuusisto, N. G. Granin, T. D. Prowse, K. M. Stewart, and V. S. Vuglinski (2000), Historical trends in lake and river ice cover in the Northern Hemisphere, *Science, 289,* 1743-1746.

McNamara, J. P., D. L. Kane, and L. D. Hinzman (1997), Hydrograph separations in an Arctic watershed using mixing model and graphical techniques, *Water Resour. Res., 33*(7), 1707-1719.

McNamara, J. P., D. L. Kane, and L. D. Hinzman (1998), An analysis of streamflow hydrology in the Kuparuk River Basin, Arctic Alaska: a nested watershed approach, *J. of Hydrol., 206,* 39-57.

McNamara, J.P., D. L. Kane, and J. E. Hobbie (2008), Hydrologic and biogeochemical controls on the spatial and temporal patterns of nitrogen and phosphorus in the Kuparuk River, Arctic Alaska. *Hydrol. Processes, 22,* 3294-3309.

Neilson, B.T., D. K. Stevens, S. C. Chapra, and C. Bandaragoda (2009), Data collection methodology for dynamic temperature model testing and corroboration, *Hydrol. Processes, 23,* 2902-2914.

Neilson, B. T., S. C. Chapra, D. K. Stevens, and C. Bandaragoda (2010a), Two-zone transient storage modeling using temperature and solute data with multiobjective calibration: 1. Temperature, *Water Resour. Res., 46,* W12520, doi:10.1029/2009WR008756.

Neilson, B. T., C. E. Hatch, H. Ban, and S. W. Tyler (2010b), Solar radiative heating of fiber-optic cables used to monitor temperatures in water, *Water Resour. Res., 46,* W08540, doi:10.1029/2009WR008354.

Osterkamp, T.E., and M.W. Payne (1981), Estimates of permafrost thickness from well logs in northern Alaska, *Cold Regions Science and Technology, 5,* 13-27.

Oswood, M.W., K. R. Everett, D. M. Schell (1989), Some physical and chemical characteristics of an Arctic beaded stream, *Holarctic Ecology, 12,* 290-295.

Rouse, W.R., M. S. V.Douglas, R. E. Hecky, A. E. Hershey, G. W. Kling, L. Lesack, P. Marsh, M. McDonald, B. J. Nicholson, N. T. Roulet, and J. P. Smol (1997), Effects of climate change on the freshwaters of Arctic and Subarctic North America, *Hydrol. Processes, 11,* 873-902.

Satoru, H., C. McCalley, K. Koba, A. E. Giblin, M. S. Weiss, G. M. Gettel, and G. R. Shaver (2006), Nitrogen fixation in surface soils and vegetation in an Arctic tundra watershed: a key source of atmospheric nitrogen, *Arctic, Antarctic, and Alpine Res., 38,* 363–372.

Serreze, M.C., J. E. Walsh, F. S. Chapin, T. E. Osterkamp, M. B. Dyurgerov, V. Romanovsky, W. C. Oechel, J. Morison, T. Zhang, and R. G. Barry (2000), Observational evidence of recent hange in the northern high-latitude environment, *Climatic Change, 46,* 159-207.

Stieglitz, M., J. Shaman, J. McNamara, V. Engel, J. Shanley, and G. W. Kling (2003), An approach to understanding hydrologic connectivity on the hillslope, *Global Biogeochemical Cycles, 17*(4), 1105, doi:10.1029/2003GB002041.

Sturm, M., T. Douglas, C. Racine, and G. E. Liston (2005), Changing snow and shrub conditions affects albedo with global implications, *J. of Geophysical Res., 110,* G01004, doi:10.1029/2005JG000013.

Theurer, F.D., K. A. Voos, and W. J. Miller (1984), Instream water temperature model, U.S. Fish and Wildlife Service, Fort Collins, Colo.

TVA (1972), Heat and mass transfer between a water surface and the atmosphere, Water Resources Research, Laboratory Report No. 14. Engineering Laboratory, Division of Water Control Planning, Tennessee Valley Authority, Norris, TN.

Vorosmarty, C., L. D. Hinzman, B. Peterson, D. Bromwich, L. Hamilton, J. Morison, V. Romanovsky, M. Sturm, and R. Webb (2001), The hydrological cycle and its role in arctic and global environmental change: A rationale and strategy for synthesis study, Arctic Research Consortium of the U.S., Fairbanks, Alaska, p. 84.

Wang, X., and J. R. Key (2003), Recent trends in Arctic surface, cloud, and radiation properties from space. *Science, 299,* 1725-1728.

Webb, B.W., D. M. Hannah, R. D. Moore, L. E. Brown, F. Nobilis (2008),. Recent advances in stream and river temperature research. *Hydrol. Processes, 22,* 902-918.

Zarnetske, J.P., M. N. Gooseff, T. R. Brosten, J. H. Bradford, J. P. McNamara, and W. B. Bowden (2007), Transient storage as a function of geomorphology, discharge, and permafrost active layer conditions in Arctic tundra streams, *Water Resour. Res., 43,* W07410, doi:10.1029/2005WR004816.

APPENDIX

Heat Balance Equations

Pool Layer 1:

$$\rho_1 C_p V_1 \frac{dT_1}{dt} = \rho_1 C_p Q_{in} T_{in} - \rho_1 C_p Q_{out} T_1 + J_{atm} A_{s,1} - \rho_1 C_p \nu_{1,2} A_{s,2} (T_1 - T_2) - \frac{K_{sed} A_{s,sed,1} (T_1 - T_{sed,1})}{z_{sed,1,2}} \quad \text{(A1)}$$

Pool Layer 2:

$$\rho_2 C_p V_2 \frac{dT_2}{dt} = J_{sn,2} A_{s,1} + \rho_2 C_p \nu_{1,2} A_{s,2} (T_1 - T_2) - \rho_2 C_p \nu_{2,3} A_{s,3} (T_2 - T_3) - \frac{K_{sed} A_{s,sed,2} (T_2 - T_{sed,2})}{z_{sed,1,2} 1.5} \quad \text{(A2)}$$

Pool Layer 3:

$$\rho_3 C_p V_3 \frac{dT_3}{dt} = J_{sn,3} A_{s,1} + \rho_3 C_p \nu_{2,3} A_{s,3} (T_2 - T_3) - \frac{K_{sed} A_{s,sed,3} (T_3 - T_{sed,3,ave})}{z_{sed,3} 0.5} \quad \text{(A3)}$$

Dividing through by ρ, Cp, and V,

Pool Layer 1:

$$\frac{dT_1}{dt} = \frac{\rho_1 C_p Q_{in} T_{in}}{\rho_1 C_p V_1} - \frac{\rho_1 C_p Q_{out} T_1}{\rho_1 C_p V_1} + \frac{J_{atm} A_{s,1}}{\rho_1 C_p V_1} - \frac{\rho_1 C_p \nu_{1,2} A_{s,2} (T_1 - T_2)}{\rho_1 C_p V_1} - \frac{K_{sed} A_{s,sed,1} (T_1 - T_{sed,1})}{\rho_1 C_p V_1 z_{sed,1,2}} \quad \text{(A4)}$$

Pool Layer 2:

$$\frac{dT_2}{dt} = \frac{J_{sn,2}A_{s,1}}{\rho_2 C_p V_2} + \frac{\rho_2 C_p \nu_{1,2} A_{s,2}(T_1 - T_2)}{\rho_2 C_p V_2} - \frac{\rho_2 C_p \nu_{2,3} A_{s,3}(T_2 - T_3)}{\rho_2 C_p V_2} - \frac{K_{sed} A_{s,sed,2}\left(T_2 - T_{sed,2}\right)}{\rho_2 C_p V_2 z_{sed,1,2} 1.5} \quad \text{(A5)}$$

Pool Layer 3:

$$\rho_3 C_p V_3 \frac{dT_3}{dt} = \frac{J_{sn,3}A_{s,1}}{\rho_3 C_p V_3} + \frac{\rho_3 C_p \nu_{2,3} A_{s,3}(T_2 - T_3)}{\rho_3 C_p V_3} - \frac{K_{sed} A_{s,sed,3}\left(T_3 - T_{sed,3,ave}\right)}{\rho_3 C_p V_3 z_{sed,3} 0.5} \quad \text{(A6)}$$

Canceling terms,

Pool Layer 1:

$$\frac{dT_1}{dt} = \frac{Q_{in}T_{in}}{V_1} - \frac{Q_{out}T_1}{V_1} + \frac{J_{atm}A_{s,1}}{\rho_1 C_p V_1} - \frac{\nu_{1,2}A_{s,2}}{V_1}(T_1 - T_2) - \frac{K_{sed}A_{s,sed,1}\left(T_1 - T_{sed,1}\right)}{\rho_1 C_p V_1 z_{sed,1,2}} \quad \text{(A7)}$$

Pool Layer 2:

$$\frac{dT_2}{dt} = \frac{J_{sn,2}A_{s,1}}{\rho_2 C_p V_2} + \frac{\nu_{1,2}A_{s,2}}{V_2}(T_1 - T_2) - \frac{\nu_{2,3}A_{s,3}}{V_2}(T_2 - T_3) - \frac{K_{sed}A_{s,sed,2}\left(T_2 - T_{sed,2}\right)}{\rho_2 C_p V_2 z_{sed,1,2} 1.5} \quad \text{(A8)}$$

Pool Layer 3:

$$\frac{dT_3}{dt} = \frac{J_{sn,3}A_{s,1}}{\rho_3 C_p V_3} + \frac{\nu_{2,3}A_{s,3}}{V_3}(T_2 - T_3) - \frac{K_{sed}A_{s,sed,3}\left(T_3 - T_{sed,3,ave}\right)}{\rho_3 C_p V_3 z_{sed,3} 0.5} \quad \text{(A9)}$$

where T = temperature (℃), Q = volumetric flow rate (m^3 day^{-1}), V = volume of the layer (m^3), ρ = density of the water (g m^{-3}), C_p = heat capacity of the water (cal g^{-1} $℃^{-1}$), A_s = surface area of each layer of the pool (m^2), ν = the vertical heat transfer coefficient (m day^{-1}), z = depth (m), K = thermal conductivity of the sediment (cal m^{-1} $℃^{-1}$ day^{-1}), J_{atm} = total surface flux (cal m^{-2} day^{-1}), and $J_{sn,i}$ = shortwave solar radiation (cal m^{-2} day^{-1}) of each layer due to attenuation. The subscripts *1*, *2*, *3*, *in*, *out*, *s*, *atm*, *sed*, and *ave* specify the top, middle and bottom layer of the pool or sediment, inflow, outflow, surface, atmospheric, sediment, and average, respectively.

Density of Water

As taken from Chapra and Martin (2004):

The density of water is related to temperature and salinity by (Millero and Poisson 1981):

$$\rho = \rho_o + AS + BS^{3/2} + CS^2$$

where ρ = density [g L^{-1}], S = salinity (ppt), and

$$a = 0.824493 - 0.0040899T + 0.000076438T^2 - 0.00000082467T^3 + 0.0000000053875T^4$$

$$b = -0.00572466 + 0.00010227T - 0.0000016546T^2$$

$$c = 0.00048314$$

in which T = temperature (^oC) and ρ_o = the density of fresh water [g L^{-1}],

$$\rho_o = 999.842594 + 0.06793952T - 9.095290\times10^{-3}T^2 + 1.001685\times10^{-4}T^3$$

$$- 1.120083\times10^{-6}T^4 + 6.536332\times10^{-9}T^5$$

The salinity is related to chloride concentration by (Thomann and Mueller 1987),

$$S = 1.80655\times10^{-3}Cl$$

where Cl = chloride concentration. The chloride concentration is related to conductivity by

$$Cl = 0 \qquad \text{Cond} < 84.2\ \mu\text{mhos}$$

$$Cl = 0.3091 \times \text{Cond} - 26.021 \qquad \text{Cond} \geq 84.2\ \mu\text{mhos}$$